Author Manuscript

Author Manuscript

Author Manuscript

Author Manuscript

HHS Public Access

Author manuscript

Nat Biomed Eng. Author manuscript; available in PMC 2022 December 21.

Published in final edited form as:

Nat Biomed Eng. 2023 April ; 7(4): 533–545. doi:10.1038/s41551-021-00736-7.

A prototype closed-loop brain–machine interface for the study and treatment of pain

Qiaosheng Zhang[1], **Sile Hu**[2], **Robert Talay**[1], **Zhengdong Xiao**[2], **David Rosenberg**[2], **Yaling Liu**[1], **Guanghao Sun**[2], **Anna Li**[1], **Bassir Caravan**[2], **Amrita Singh**[1], **Jonathan D. Gould**[3], **Zhe S. Chen**[2,4,5,*], **Jing Wang**[1,4,5,*]

[1]Department of Anesthesiology, Perioperative Care and Pain, New York University School of Medicine, New York, NY 10016, USA

[2]Department of Psychiatry, New York University School of Medicine, New York, NY 10016, USA

[3]College of Arts and Sciences, New York University, New York, NY 10003, USA

[4]Department of Neuroscience & Physiology, New York University School of Medicine, New York, NY 10016, USA

[5]Neuroscience Institute, New York University School of Medicine, New York, NY 10016, USA

Abstract

Chronic pain is characterized by discrete pain episodes of unpredictable frequency and duration. This hinders the study of pain mechanisms, and contributes to the use of pharmacological treatments associated with side effects, addiction and drug tolerance. Here, we show that a closed-loop brain–machine interface (BMI) can modulate sensory-affective experiences in real time in freely behaving rats by coupling neural codes for nociception directly with therapeutic cortical stimulation. The BMI decodes the onset of nociception via a state-space model on the basis of the analysis of online-sorted spikes recorded from the anterior cingulate cortex (which is critical for pain processing), and couples real-time pain detection with optogenetic activation of the prelimbic prefrontal cortex (which exerts top–down nociceptive regulation). In rats, the BMI effectively inhibited sensory and affective behaviors caused by acute mechanical or thermal pain, and by chronic inflammatory or neuropathic pain. The approach provides a blueprint for

Reprints and permissions information is available at www.nature.com/reprints.

[*]**Correspondence and requests for materials** should be addressed to C.S.Z. and J.W. Corresponding authors: zhe.chen@nyulangone.org; jing.wang2@nyulangone.org.

Author contributions

J.W. and Z.S.C. conceived and designed the study; Q.Z. designed the 3D drive, performed the surgeries, implemented the BMI hardware system. Q.Z., S.H., R.T., A.S., B.C., Z.X., D.R., Y.L., G.S., A.L., and J.D.G. collected the data; Q.Z., A.S., Z.X., J.D.G., and R.T. analyzed the data; S.H., Z.X., Q.Z., and Z.S.C. contributed to BMI software development; J.W., Z.S.C., supervised the project; J.W. and Z.S.C. wrote the manuscript with input from other authors.

Competing interests

The authors declare no competing interests.

Code availability

The custom BMI client software used in this study is available at https://github.com/wangresearch1/onlinePainDecodingGUI.

Supplementary information is available for this paper at https://doi.org/10.1038/s41551-021-00736-7.

Peer review information *Nature Biomedical Engineering* thanks the anonymous, reviewer(s) for their contribution to the peer review of this work.

Author Manuscript Author Manuscript Author Manuscript Author Manuscript

demand-based neuromodulation to treat sensory-affective disorders, and could be further leveraged for nociceptive control and to study pain mechanisms.

Chronic pain affects one in four adults, and it is composed of discrete episodes of acute pain that are triggered by external stimuli or occur spontaneously[1]. Currently, there is no method to isolate individual symptomatic episodes, making it difficult for the study of pain mechanisms, especially the mechanisms of spontaneously occurring pain, and for treatment. Pain treatment, therefore, depends on continuous pharmacological delivery or neurostimulation. Around-the-clock pharmacological treatment for chronic pain is linked with sedation, desensitization and even addiction[2,3]. Meanwhile, continuous spinal cord stimulation is associated with side effects such as numbness and paresthesia[4], whereas brain targets serve a multitude of functions, making continuous stimulation impractical to implement, with questionable long-term benefits[5–31]. Therefore, a key challenge in the study and management of chronic pain is to aim treatment at specific symptomatic episodes to minimize side effects of overuse and to improve compliance.

A closed-loop BMI couples automated detection of neural signals for behavior with therapeutic neuromodulation and has shown promise for seizure control and motor rehabilitation[32–46]. Recent advances in optogenetics and *in vivo* electrophysiology enable closed-loop control of discrete neural circuits for mechanistic and treatment studies in experimental models[47,48]. However, the application of closed-loop BMI remains highly speculative in sensory-affective disorders, due to challenges in real-time sensory decoding and direct behavioral control in awake experimental subjects. We hypothesize that by coupling pain episodes detected by automated analysis of neural activity with therapeutic brain stimulation, a closed-loop BMI can deliver demand-based analgesia to minimize overuse and improve safety. Just as importantly, this interface can be used for studies of pain mechanisms, especially mechanisms of spontaneous pain or tonic pain, which currently cannot be reliably assessed.

The design of a closed-loop BMI requires an input arm for signal detection and an output arm for treatment (Fig. 1). The challenge with the design of a BMI for pain control is that unlike visual or auditory systems, there is no primary pain cortex. Instead, multiple cortical regions are involved in processing and regulating pain. A wealth of human neuroimaging and lesioning data, as well as animal data, have indicated that the anterior cingulate cortex (ACC) is critical for pain processing[49–65]. Supervised or unsupervised learning methods have shown that neural signals from the ACC, including spike activities, can distinguish the intensity and timing of noxious inputs with good sensitivity and specificity[57–59,66]. Thus, neural activity recorded from the ACC could be used for pain detection in the design of a prototype BMI approach. For the treatment output arm, we sought brain targets that could provide endogenous pain relief. Activation of these regions with a BMI in a temporally regulated manner presumably could provide additional pain relief while minimizing side effects. Recent work from multiple groups has shown that pyramidal neurons in the prelimbic region of the PFC project to regions such as the nucleus accumbens, amygdala and periaqueductal gray to exert endogenous relief of sensory and affective behaviors associated with acute and chronic pain in rodent models[67–76]. Meanwhile, prior unbiased machine

Author Manuscript Author Manuscript Author Manuscript Author Manuscript

learning analyses also revealed that neural firing rates in the prelimbic PFC could distinguish noxious from non-noxious peripheral stimuli with up to 75% accuracy, further supporting the specificity of the nociceptive response in this region[72]. The rodent prelimbic PFC shares functional and structural homology with the dorsolateral PFC in primates[76,77]. Previous studies have shown that functional deficits in the dorsolateral PFC play a significant role for the pathogenesis of chronic pain, and this region will likely serve as a key neuromodulation target in patients[78]. Therefore, to facilitate translation, we have selected the PFC as the treatment arm in the development of the pain-modulating BMI.

Results

Design of a closed-loop BMI to study and treat pain.

To develop a closed-loop BMI for pain, we paired a detection arm with a treatment arm (Fig. 1a). We used neural activity recorded from the ACC for pain detection in the current design, given its critical role in pain processing (Fig. 1b and Supplementary Fig. 1a)[49–65]. Decoding the onset and duration of a sensory or aversive event in real time in an awake, freely behaving animal or human subjects requires a statistical model to detect changes in neural responses in the presence of background noise. We have developed a state-space model (SSM) to analyze the onset of changes in ensemble spike activity in the ACC in response to noxious stimuli (see Methods; Fig. 1c, and Supplementary Fig. 1d). With this SSM-based strategy, we identify a proxy for the acute pain signal that drives the observed population spike activity, thus formulating pain onset detection as detection of a change from the putative baseline condition. This model-based strategy has revealed that the latent processes driving ACC neuronal activities correlate to the onset of observed pain behavior with high degrees of accuracy and temporal precision[57,58]. Here, we have adapted this SSM-based strategy for real-time detection of the onset and duration of nociceptive responses in the ACC from awake, freely behaving rats (Fig. 1). For the treatment arm, we used optogenetic activation of the prelimbic PFC, a region that has been shown to provide top-down pain regulation[67–76], in our current BMI design (Supplementary Fig. 1b, c). To assist online model parameter selection and data visualization, we designed a custom graphic user interface (GUI) to integrate the pain detection arm with the treatment arm, forming a closed-loop neural interface (Supplementary Fig. 1c, e).

Closed-loop BMI controls acute evoked pain.

We first applied this real-time BMI in the context of acute thermal pain. We used a calibrated infrared (IR) generator from the Hargreaves pain assessment toolkit to deliver a noxious stimulus at high IR intensity, and a non-noxious stimulus at low IR intensity to the hind paws of rats (Fig. 2a, b). As shown previously, ACC neurons contralateral to the site of peripheral stimulation increased their firing rates in response to the noxious thermal stimulus (Supplementary Fig. 2a, c–e)[59]. In contrast, the non-noxious stimulus did not produce significantly increased spiking activities in the same neurons (Supplementary Fig. 2b–e). We applied our SSM decoding method to detect the onset of nociceptive ACC neuronal responses in real time (Fig. 1c, and Supplementary Fig. 1c). Our model-based strategy detected the onset of pain-induced responses reliably after the presentation of noxious stimulus, with high temporal precision (Fig. 2c). The SSM-based decoder detected

Author Manuscript Author Manuscript Author Manuscript Author Manuscript

up to 80% evoked thermal pain episodes, with relatively low false detection rates (Fig. 2d, e, and Supplementary Table 1). In a majority of the cases, detection occurred after the presentation of noxious stimulus but prior to paw withdrawals, suggesting that cortical nociceptive response precedes behavioral response (Fig. 2c, f, g). These results validate the accuracy of our pain-onset decoder and the possibility for a closed-loop system to intervene in pain-related behaviors immediately after the detection of cortical nociceptive responses. Thus, we coupled this detection of nociceptive activity triggered by the SSM with optogenetic stimulation of the prelimbic PFC contralateral to the ACC recording sites (Fig. 1 and Supplementary Fig. 1a, b). We expressed ChR2 (or YFP control) using a CaMKII promotor to activate pyramidal neurons in the prelimbic PFC (Supplementary Fig. 1b). We applied our closed-loop BMI to the Hargreaves test of acute thermal pain (Fig. 2f). Our results showed that the BMI treatment prolonged withdrawal latency on the Hargreaves test, indicating relief of pain-related behavior (Fig. 2h). We then compared the pain-inhibitory effect provided by the BMI with that provided by manually controlled, continuous PFC activation. We found that BMI-triggered PFC activation was as efficacious as continuous PFC activation in reducing thermal sensitivity on the Hargreaves test, further validating the capability of this closed-loop neuromodulation system to inhibit pain (Fig. 2h). At the cellular level, activation by BMI reduced the peak and cumulative firing rates of ACC pain responsive neurons after noxious stimulations (Fig. 2i–k). This temporally specific reduction in ACC neuronal activity confirms the causal effect between ACC firing activity and pain behaviors that has been suggested in previous studies[53,59]. Therefore, a closed-loop BMI can not only deliver therapeutic interventions in real time, but also enable studies of causal inference for the neural basis of pain.

Next, we used pin prick (PP) to deliver mechanical pain to the hind paws of rats (Fig. 3a, b). In contrast to IR, PP caused almost instantaneous withdrawal response. Nevertheless, ACC neurons increased their firing rates in response to noxious stimulations (Supplementary Fig. 3a, c–e), in contrast to non-noxious stimulations (von Frey filaments, or vF) (Supplementary Fig. 3b–e), and our SSM-based decoder was able to detect these evoked mechanical pain episodes (Fig. 3c–e, and Supplementary Table 1).

Pain is characterized by both sensory and affective components. To test the affective component of pain, we used a classic conditioned place aversion (CPA) assay to assess the ability of the BMI to control the aversive response to mechanical pain[59,72,79,80]. During the conditioning phase, we applied noxious stimulations (PP) to the rats' hind paws in both treatment chambers (Fig. 3f). In one of these chambers, rats received automated, BMI-triggered therapeutic PFC activation. In the opposite chamber, rats received randomly delivered PFC stimulations of matching duration and intensity. After conditioning, rats preferred the chamber associated with the BMI treatment (Fig. 3g). Similarly, rats preferred BMI-triggered PFC activation to no PFC activation (Supplementary Fig. 4a, b). In contrast, control rats that did not express ChR2 did not develop chamber preference (Fig. 3h, i). Further, conditioning with randomly delivered optogenetic PFC stimulation did not result in chamber preference (Supplementary Fig. 4c, d), suggesting that context-specific activation of the prelimbic PFC is important for providing pain relief. To rule out potential cognitive and affective side effects of PFC stimulation associated with BMI, we tested the preference for the BMI in control rats where a non-noxious stimulus (a 6g von Frey, or vF, stimulus)

Author Manuscript Author Manuscript Author Manuscript Author Manuscript

was presented in both chambers (Supplementary Fig. 5a, b). In the absence of noxious stimuli, rats did not develop a preference for the BMI treatment, indicating that PFC stimulation delivered by the BMI was not intrinsically rewarding or aversive. Furthermore, BMI did not alter locomotion (Supplementary Fig. 5c). Therefore, a closed-loop system coupling detected nociceptive responses in the ACC with therapeutic PFC activation specifically inhibits both sensory and affective behavioral response to acute noxious stimuli.

Closed-loop BMI controls chronic pain.

Next, we investigated whether this closed-loop BMI could be used to inhibit chronic pain. Two hallmark features of chronic pain are hypersensitivity to peripheral stimuli and tonic or spontaneous pain. We first assessed hypersensitivity in a well-established inflammatory pain model (Complete Freund's Adjuvant or CFA model, Fig. 4a). As expected[59], CFA-treated rats developed sensory allodynia to mechanical von Frey filament (vF) stimulations, as manifested by paw withdrawal responses (Fig. 4b and Supplementary Fig. 6a). Our neural decoding analysis distinguished a 6g vF stimulus that sufficiently elicited nocifensive withdrawals from a 0.4g vF stimulus that did not elicit withdrawals (Fig. 4c–e and Supplementary Table 1). These results indicate that in addition to detecting events triggered by noxious stimuli, our SSM-based strategy can also detect allodynia events in real time. BMI-triggered activation of the prelimbic PFC, meanwhile, reduced mechanical allodynia (Fig. 4f). In addition to peripheral hypersensitivity at the site of injury, chronic pain also causes an increased aversive response, which can be assessed by the CPA[59,68,72,79,80]. In one chamber, we paired a peripheral 6g vF stimulus (which is sufficient to induce allodynia) with BMI-driven activation of the PFC, and in the opposite chamber paired this stimulus with randomly delivered PFC activation (Fig. 4g). After conditioning, rats preferred the BMI-paired chamber (Fig. 4h–j). In contrast, rats did not prefer the BMI-paired chamber when they received a non-noxious, 0.4g vF stimulus during conditioning (Supplementary Fig. 6b, c). We then repeated these experiments in a model of chronic neuropathic pain (Spared Nerve Injury or SNI)[67,81] (Fig. 5a, b and Supplementary Fig. 7a). Again, our SSM-based strategy could detect when rats received a 6g vF stimulus that elicited nocifensive withdrawals, versus when rats received a 0.4g vF stimulus that did not consistently elicit withdrawals (Fig. 5c–e and Supplementary Table 1). The BMI, driven by pain detection, in turn reduced mechanical allodynia in the SNI model (Fig. 5f). In the CPA assay, we paired the 6g vF stimulus with either BMI-triggered or random PFC activation (Fig. 5g), and SNI-treated rats preferred the BMI-paired chamber (Fig. 5h–j). In contrast, rats showed no preference for the BMI-paired chamber if the peripheral stimulus was non-noxious (Supplementary Fig. 7b, c). Together, these results demonstrate that peripheral allodynia in the chronic pain state produces similar neural responses in the ACC as acute noxious stimulations in naïve animals, and these neural responses can in turn be used to trigger closed-loop neurostimulation to inhibit sensory hypersensitivity and decrease aversion.

In addition to hypersensitivity to evoked stimuli, a key symptom for chronic pain is tonic pain[80]. Recent studies have shown that the CPA assay can be used to specifically test the presence of tonic pain in animal models[67,80,82,83]. However, the identification of discrete spontaneously occurring pain-aversive episodes that underlie tonic pain remains an unmet challenge in both animal and human research. This challenge hinders the understanding

Author Manuscript Author Manuscript Author Manuscript Author Manuscript

of neural mechanisms for tonic pain and the development of appropriate therapeutics. The high temporal precision of the closed-loop BMI provides a solution to this problem. A number of studies have demonstrated the critical role of ACC neurons in mediating the tonic-aversive quality of chronic pain[52,53,59,84]. Thus, we hypothesized our decoding algorithm could be triggered by spontaneously occurring nociceptive signals in ACC. To detect such signals, we inferred state-space model parameters based on population ACC activities during training trials from evoked pain episodes, and then applied these parameters to isolate putative spontaneous pain episodes based on dynamic changes in ACC activities in freely-moving rats from chronic pain models (see Methods). The accuracy of these detected episodes could then be tested by the application of BMI on pain behaviors in the CPA assay. In CFA-treated rats, we paired one CPA chamber with BMI, and the other chamber with random activation of the PFC of matching duration and intensity, in the absence of additional peripheral stimulations (Fig. 6a). Detected nociceptive activity in the ACC should trigger PFC activation to inhibit pain-related behaviors during a prolonged conditioning phase[85]. As we expected, after training with an evoked stimulus, our decoder identified putative spontaneous pain episodes in the CFA model (Fig. 6b and Supplementary Fig. 8). After conditioning, rats developed preference for the chamber associated with BMI-triggered PFC activation, suggesting that our BMI could identify and treat spontaneous pain (Fig. 6c–e). These results support the role of the ACC neurons to process the aversive signal in tonic pain conditions as shown in previous studies[52,53,59,84]. To rule out the potential rewarding effects of BMI, we tested the preference for the BMI in naive rats, and found that these control rats did not develop a preference for the BMI treatment (Supplementary Fig. 9).

Next, we tested the ability of the BMI for targeting tonic neuropathic pain in the SNI model (Fig. 7a). Our SSM-based strategy provided similar spontaneous nociceptive detection in the SNI model (Fig. 7b), and rats showed preference for the BMI treatment, suggesting that our closed-loop BMI could inhibit tonic pain (Fig. 7c–e). As PFC activation triggered by detected ACC nociceptive response induces pain relief compared with random activation, the detected activity has a high likelihood of underlying true spontaneous pain events. Therefore, our BMI can serve as a valuable tool for identifying spontaneously occurring pain for mechanistic inquiries. To validate the capability of our BMI to detect and modulate tonic pain, we examined its efficacy at inhibiting paw-licking behaviors. Paw licking has been identified as a spontaneous pain-related behavior in inflammatory pain models[86–89]. Here we found that the closed-loop BMI was effective in reducing the paw-licking frequency and duration in the CFA model (Supplementary Fig. 10). These results further support the efficacy of the closed-loop BMI to detect and treat tonic pain in rodent models.

Discussion

To date, treatment options for chronic pain remain limited, and continuous pharmacological and neuromodulation therapies are associated with multiple side effects. Here we have engineered a BMI as a prototype closed-loop neuromodulation system to inhibit pain. This system can be used to test therapeutics and to provide causal inference for mechanisms of nociception. It can be further developed to deliver demand-based pain treatment in patients. A major advantage of this system is its ability to provide high temporal resolution to

Author Manuscript Author Manuscript Author Manuscript Author Manuscript

precisely target discrete symptomatic episodes. By tailoring transient brain stimulation with specific pain episodes, this BMI can minimize over-treatment to improve compliance and reduce side effects for patients who need long-term therapies.

In our study, we have chosen the ACC as the detection arm and the PFC as the treatment arm. The choice of ACC for pain detection is based on its well-established function in pain processing[49–65,90], as well as previous success in determining the intensity and timing of pain based on pre-recorded neural activities in this region[57–59,66]. Our results here validate the important role of the ACC to signal the onset and duration of pain, compatible with previous reports[52,53,59,84]. Future studies can further refine the detection sensitivity for spontaneously occurring pain, by scaling up or down the coefficients of our model-based decoding algorithm, or by combining recordings from additional neural regions. Future investigations can also examine in greater detail how pain decoding in the ACC correlates with pain identification using behavioral analyses[91,92]. In our study, we have targeted the prelimbic PFC as the treatment arm, as previous studies have shown that this region provides critical top-down projections for endogenous pain inhibition[67–71]. Our behavioral results validate the role of this region in the regulation of both sensory withdrawal and pain-related aversion. Our results further showed that transient activation of the PFC is sufficient to reduce pain symptoms, as long as neuromodulation is temporally coupled with nociceptive inputs. Given well-established structural and functional homology between the rodent prelimbic PFC and the dorsolateral PFC in humans[76,77], our prototype BMI provides the intriguing potential for effective demand-based treatment in patients.

Like many cortical areas, the ACC and PFC have multiple functions in addition to pain processing and regulation. Since currently we do not have specific anatomic targets for pain treatment, most brain regions that can be used as components of a practical closed-loop BMI will inevitably have nonspecific effects. Similarly, nonspecific effects are associated with current neuromodulation treatments such as deep brain stimulation treatments for Parkinson's disease or mood disorders[93,94]. However, a BMI approach can reduce these side effects by restricting these nonspecific effects to the duration of treatment, which in turn is limited to only when the brain senses pain. Thus, in our study we propose a method to improve pain treatment specificity in terms of time and context, and this approach can complement future efforts to achieve further specificity through improved spatial, anatomic and cellular resolution.

While we have used the ACC and PFC in the development of our pain BMI, our system has the flexibility to operate with other cortical or subcortical targets. For example, activities in the primary somatosensory cortex, the insular cortex, the thalamus, and amygdala, can all form detection arms in this BMI, and a comparison of BMI-mediated behavioral control will quantify the specific contribution of individual regions to pain processing. While false and missed detections can be caused by non-specificity and/or non-stationarity of neuronal firing in specific brain regions of freely behaving rats, simultaneous recordings across multiple pain-processing regions in the brain, such as the ACC, the primary somatosensory cortex and the insular cortex, have the potential to further improve decoding accuracy, especially for spontaneously occurring pain episodes[95]. Meanwhile, additional pain-regulating regions such as the primary motor cortex and the periaqueductal gray can also be tested as the

Author Manuscript Author Manuscript Author Manuscript Author Manuscript

therapeutic arm of this BMI. Future work in these and other cortical and subcortical regions shall be done to further validate and refine our BMI design. In addition, our neural interface can be applied to causal investigations of real-time neural changes across multiple brain regions for pain processing and regulation as well as investigations of laterality of cortical pain processing.

To further facilitate clinical translation, future work should also focus on the use of other recording modalities, including local field potentials, electrocorticography or electroencephalogram signals, as well as the deployment of wireless electrical or ultrasound stimulations. These future developments of the BMI technology will be particularly beneficial for patients who suffer from chronic pain, such as patients with chronic neuropathic back pain or fibromyalgia, whose symptoms can be triggered by specific peripheral stimuli such as positional changes but may also occur spontaneously. Pain in these patients are unpredictable and, in some cases, lacking anatomic specificity, making continuous neuromodulation difficult to implement. As our study demonstrates, BMI technology has the potential to capture these symptomatic pain episodes and provide temporally targeted therapy to minimize over-treatment.

In summary, we have designed a closed-loop BMI to study and treat acute and chronic pain in freely behaving experimental models. Our results provide evidence of feasibility for the BMI technology to target sensory and affective processes associated with neuropsychiatric diseases, both as a system for mechanistic inquiry and as a blueprint for therapy.

Methods

Experimental protocol, data acquisition and BMI system architecture.

All experimental studies were performed in accordance with the New York University School of Medicine (NYUSOM) Institutional Animal Care and Use Committee and the National Institutes of Health (NIH) *Guide for the Care and Use of Laboratory Animals* to ensure minimal animal use and discomfort. Male Sprague-Dawley rats were purchased from Taconic Farms and kept at the vivarium facility in the NYU Langone Science Building, with controlled humidity, temperature, and 12-hr (6:30 AM–6:30 PM) light-dark cycle. Food and water were available ad libitum. Animals weighed 250 to 300 g upon arrival to the facility and were given 10 days on average to adjust to the new environment before initiation of experiments.

Virus construction and packaging.

Recombinant AAV vectors were serotyped with AAV1 coat proteins and packaged at the UPenn vector core. Viral titers were 5×10^{12} particles per mL for AAV1.CaMKII.ChR2-eYFP.WPRE.hGH, and AAV1. CaMKII(1.3).eYFP.WPRE.hGH.

Viral injection.

Rats were anesthetized with isoflurane (1.5 to 2%). In all experiments, virus was delivered to the prelimbic PFC only. Rats were unilaterally injected with 0.5 μL of viral vectors at a rate of 0.1 μL every 20 s with a 26-gauge 1 μL Hamilton syringe at anteroposterior (AP)

Author Manuscript Author Manuscript Author Manuscript Author Manuscript

+2.9 mm, mediolateral (ML) ±1.6 mm, and dorsoventral (DV) −3.7 mm, with tips angled 17° toward the midline. The microinjection needles were left in place for an additional 10 min, raised 1 mm, and left for another minute to allow for diffusion of virus particles away from injection site and to minimize spread of viral particles along the injection tract. After viral injections, the scalp was sutured and given three weeks for viral expression before optic fiber and electrode implantation.

Prelimbic PFC optic fiber and ACC silicon probe implantation surgery.

Optic fiber and electrode implants were performed as described in previous studies[59,72]. We constructed custom fiber optic cannulae with 200 μm optic fibers held in 2.5 mm ferrules (Thorlabs) for prelimbic PFC optogenetic stimulation. 32-channel silicon probes (Buzsaki32-H32_21 mm, NeuroNexus Technologies) were implanted in the ACC for neural recording in this study. Silicon probes were glued with 3D printed custom design drives or commercial dDrives (NeuroNexus Technologies) before implantation. During the implant, rats were anesthetized with isoflurane (1.5 to 2%). Optic fibers were implanted 0.5 mm right above prelimbic PFC viral injection spot (AP +2.9 mm, ML ±1.6 mm, DV −3.2 mm), with tips angled 17° toward the midline. Contralateral to the optical fiber implant, silicon probes were implanted in the ACC (AP +2.7mm, ML±1.6 mm, DV −2.0 mm) with tips angled 20° toward the midline. Silicone artificial dura gel (Cambridge NeuroTech) was added to protect the dura. Vaseline was used for wrapping electrode movable parts, which include silicon probe shanks and flexible cables, and drive shuttle. Both optical fiber and drive were secured to the skull screws with dental cement. After surgery, rats were given one week to recover before neural recordings.

In vivo electrophysiological recordings and optogenetic stimulation.

The hardware of the BMI system for pain experiments consists of following components: electrode arrays (with drives) and headstages, commutator, data acquisition system, Optic fiber cannulas, blue laser, desktop computer, video cameras and other optional devices, as shown in Fig. 1 and Supplementary Fig. 1.

Animals with chronic optical fiber and electrode implants were given a 30 min period to habituate to a recording chamber over a mesh or glass table before recording. Silicon probes were connected with 32-ch digital headstages (HST/32D, Plexon) and wired through a motorized commutator (OPT/Carousel M Commutator 2LED-4DHST-TH, Plexon). Optic fiber cannulas were connected with a 465nm blue laser through mating sleeves (ADAF2, Thorlabs) and fiber patch cables. The blue laser was magnetically mounted on the same carousel commutator.

Neural signals were recorded through a 64-ch OmniPlex data acquisition system (Plexon). The neural signals used for model-based pain detection were spiking rates of individual neurons. Online sorted neural spikes from individual neurons and raw, unfiltered wide band signals were recorded at 40 kHz sampling rate. Online sorted spike timestamps were used for real-time close-loop pain onset detection. Raw wide band signals were saved for offline sorting and further data analysis. In addition, real-time pain onset decoding timestamps,

Author Manuscript Author Manuscript Author Manuscript Author Manuscript

synchronized nociceptive stimuli or control stimuli timestamps, and autonomous triggered blue laser onset timestamps were all recorded as digital events in the raw data.

The spikes were thresholded from high-pass filtered (>300 Hz) raw neural signals and further online spike sorted through 2D Polygon method (PlexonControl, Plexon). Only spikes with high signal-to-noise ratio (SNR>3) were selected for BMI population decoding. Online sorted spike time events were packaged and sent to BMI client software through Plexon application program interfaces with 50-ms bin size. The state space model would calculate the output inference of current latent variable based on the binned spike counts. The model would trigger an optogenetic stimulation if the threshold criteria was met. In the meantime, the raw neural signals, online sorted spikes, multiple event time stamps which included pain stimulus events, pain onset detection events, optogenetic stimulus events were recorded through PlexControl (Plexon) for further offline data analysis.

For optogenetic stimulation, the blue laser was controlled by OmniPlex digital 5V TTL output. The optic fiber tip output power was calibrated before experiments. The parameters for optogenetic stimulation were 20 Hz with 10-ms pulse width, of 5-s duration. For control experiments, during Hargeaves' test, an experimenter manually turned on PFC stimulation continuously whenever a thermal stimulus was applied[67].

During recording, three video cameras (DMK23U, Imaging Source, FDR-AX53, Sony) were used to record rat behavior and BMI client software online-decoding results. The cameras were synchronized with neural recording at the beginning of each recording session. Long inter-trial intervals between trials were used to avoid behavioral or neural sensitization.

State-space method for detecting the onset of pain signals.

Pain perception is a dynamic process, and the pain percept can be modeled as an abstract latent variable. In our previous work, we have formulated the problem of detecting the onset of pain signals as a change-point detection problem[57,58]. The detection problem was resolved by a state-space analysis, where the state-space model (SSM) consists of a state equation and a measurement equation[96]. In the state equation (1), we assumed that the temporal neural activity $\boldsymbol{y}_k$ (k=1,…,K), represented by a C-dimensional vector, was driven by a common one-dimensional latent Markovian process z_k:

$$z_k = a z_{k-1} + \epsilon_k \tag{1}$$

where ϵ_k specifies a temporal Gaussian prior (with zero mean and variance σ^2) on the latent process, and $0<|a|<1$ is the first-order autoregressive (AR) coefficient. In the measurement equations (2, 3), we assumed the Poisson linear dynamical system (PLDS) for neuronal ensemble spikes, with the observation vector $\boldsymbol{y}_k$ consisting of spike count of C neurons (bin size Δ), where the logarithm of the neuronal firing rate, $\boldsymbol{\eta}_k$, is modulated by a weight factor in vector $\boldsymbol{c}$ plus a DC term $\boldsymbol{d}$

$$\boldsymbol{\eta}_k = \boldsymbol{c} z_k + \boldsymbol{d} \tag{2}$$

Author Manuscript Author Manuscript Author Manuscript Author Manuscript

$$\boldsymbol{y}_k \sim Poisson(\exp(\boldsymbol{\eta}_k)\Delta) \tag{3}$$

The modulation parameter in the vector $\boldsymbol{c}$ determines the modulation degree of each neuron. A high absolute value of the modulation indicates that the neuron is likely to be pain-modulated. The second equation is a generalized linear model (GLM) that employs an exponential link function through $\boldsymbol{\eta}_k$, where $\boldsymbol{y}_k$ is Poisson distributed with the rate parameter $\exp(\boldsymbol{\eta}_k)$.

During the training phase, we have developed an iterative expectation maximization (EM) algorithm to infer latent state sequences (E-step) and unknown parameters Θ, where Θ={a, c, d, σ^2} (M-step). This model estimation was completed in a few calibration trials at the beginning of each BMI experiment. We used evoked pain trials in training, since the parameter $\boldsymbol{c}$ reflects the degree of pain modulation for each neuron. Data from baseline alone was not sufficient to infer the pain-modulation coefficients for pain-modulated neurons. However, the parameter $\boldsymbol{a}$ and $\boldsymbol{d}$ could be estimated from the baseline without evoked pain trials, or could be updated from time to time through the interactive graphic user interface (GUI).

Upon model identification, in the testing trials, an online recursive filter was run to estimate the latent state estimate $\hat{z}_k$[57,58]. Specifically, the recursive filtering operations consisted of a prediction step (equations 4–6) and an update step (equations 7 and 8) as follows:

$$\hat{z}_{k|k-1} = a\hat{z}_{k-1|k-1} \tag{4}$$

$$Q_{k|k-1} = a^2 Q_{k-1|k-1} + \sigma^2 \tag{5}$$

$$\hat{\boldsymbol{y}}_{k|k-1} = \exp(\boldsymbol{c}\hat{z}_{k-1|k-1} + \boldsymbol{d})\Delta \tag{6}$$

$$Q_{k|k}^{-1} = Q_{k|k}^{-1} + \boldsymbol{c}^{\mathrm{T}}\, diag(\hat{\boldsymbol{y}}_{k|k-1})\boldsymbol{c} \tag{7}$$

$$\hat{z}_{k|k} = \hat{z}_{k|k-1} + Q_{k|k}\boldsymbol{c}^{\mathrm{T}}(\boldsymbol{y}_k - \hat{\boldsymbol{y}}_{k|k-1}) \tag{8}$$

where $Q_{k|k-1}$ and $Q_{k|k}$ denote the predicted and filtered state covariance matrices, respectively. The posterior state variance was derived from a Gaussian approximation of the log-posterior, which is the sum of a log-Gaussian prior and a log-Poisson likelihood[97]. We then used the filtered latent state estimate $\hat{z}_{k|k}$ to compute the Z-score related to the baseline (equation 9) and further converted it to probability or one-tailed P-value[23]. We monitored the probability to assess the significance of change point detection. The criterion of Z-score change was determined by a critical threshold for reaching statistical significance. The first time point that crossed the significance threshold for the change point was treated as the onset of pain. Using 95% significance level, it was concluded that when Z-score–CI >

Author Manuscript Author Manuscript Author Manuscript Author Manuscript

1.65 or Z-score + CI < −1.65, where the CI denotes the confidence interval derived from the state posterior variance.

$$\text{Z_score} = \frac{z - \text{mean}(z_{\text{baseline}})}{\text{SD}(z_{\text{baseline}})} \tag{9}$$

The same decoding strategy for acute pain was used to detect putative spontaneous pain, where we trained the model parameter $\boldsymbol{c}$ 1-3 trials prior to detection.

BMI software development.

The BMI software that manages the operation of the system was run on a desktop PC (Intel Xeon E5-1620 CPU, 3.5 GHz, 48 GB memory, Window OS). The software supported the hardware system for online neural decoding analysis and the graphic user interface (GUI).

The components and tasks of the BMI system was managed by a client software including the following modules: (i) data acquisition and buffering, (ii) online neural encoding/decoding algorithms, (iii) external device control, (iv) configuration management, and (v) user interfaces. We developed the software in C/C++ programming language along with the software developing toolkit provided by Plexon and other open-source software packages. To accommodate maximum flexibility while minimizing the complexity of maintenance, the functional modules in the software were designed with encapsulation for decoupling purposes.

Proper buffering was required for both the streaming neural signals and the decoding analysis results. In online BMI experiments, although the total recording time lasted for an hour or more, only the recent recorded data contributed to the detection analysis (e.g. computation of Z-score and its confidence intervals) of the current time point. Therefore, we used a small buffer space to store the newest data and updated the buffer when new data arrived. To minimize the data transfer cost in the buffer space, we used a circular buffering strategy; namely, the newest data always overwrote the oldest one.

The software consists of multiple task threads[98]. In order to avoid the mutual blocking between multiple tasks, we assigned different tasks on multiple threads running in parallel. The task threads included the acquisition thread, training threads, online decoding threads, user interface (UI) thread and external device controlling thread (Supplementary Fig. 1d). A custom GUI was designed and managed by the UI thread, allowing the visualization of the streaming neural signals as well as the response for user operations (Supplementary Fig. 1e).

Complete Freund's Adjuvant (CFA) administration.

To induce chronic inflammatory pain, 0.1 mL of CFA (*Mycobacterium tuberculosis*, Sigma-Aldrich) was suspended in an oil saline 1:1 emulsion and injected subcutaneously into the plantar aspect of the hind paw. CFA injections were administered into the paw that was contralateral to implanted recording electrodes.

Author Manuscript Author Manuscript Author Manuscript Author Manuscript

Spared nerve injury (SNI) procedure.

SNI procedure was performed as described previously[99]. After rats were anesthetized with isoflurane (1.5 to 2%), the skin on the lateral surface of the thighs was incised. The bicep femoris was dissected to expose the sciatic nerve and its three terminal branches: sural, common peroneal, and tibial nerves. The common peroneal and tibial nerves were tied off with nonabsorbent 5-0 silk sutures at the proximal point of the trifurcation, and then cut distal to each knot to prevent reattachments. The muscle layer was then sutured closed with 4-0 absorbable sutures and the skin was sutured closed with 3-0 silk sutures. SNI procedure was performed on the side contralateral to implanted recording electrodes.

Hargreaves Test (Plantar Test).

The Hargreaves test was performed to evaluate the rats' response to acute thermal stimulation. A mobile radiant heat-emitting device with an aperture of 10 mm (37370 plantar test, Ugo Basile) was used to produce acute thermal stimulation of the plantar surface of the hind paw. The rats were placed in a plexiglass chamber over a Hargreaves glass table and allowed to habituate. An average of at least 5 trials were performed to measure the latency to paw withdrawal for each testing condition. This latency was automatically recorded, and an average latency across the trials was computed. Paw withdrawals resulting from locomotion or weight shifting were not counted and the trials were repeated in such cases. Measurements were repeated at approximately 5-min intervals. An IR intensity of 70 was used to provide noxious stimulation, and IR intensity of 10 was used as control for non-noxious thermal stimulation that was not noxious. IR stimuli were terminated by paw withdrawals or held continuously for 5 s.

For online BMI experiments, the SSM was first trained with 1-5 trials ("calibration trials") of noxious stimulus at the beginning of the experiment. Following training, an average of at least 5 trials were performed with activation of the BMI to test the efficacy of the BMI in inhibiting peripheral pain response. Measurements were repeated at 3-5 min intervals.

Mechanical pain detection.

Rats with optic fiber and silicon probe implants were given 30 min to habituate in a plexiglass chamber over a mesh table. The SSM was trained using a noxious stimulus (pin prick, or PP, in naive rats, and 6g von Frey filaments, or vF, in CFA- or SNI-treated rats). The noxious stimulus was applied to the plantar surface of the hind paw contralateral to the ACC recording site in freely moving rats. Noxious stimulations were terminated by paw withdrawal. Following model training, a period of rest was given the rats to avoid behavioral or neural hypersensitivity. A total of 20-25 trials were then performed with each stimulus (equal number for each stimulation type with variable inter-trial intervals) to generate spike raster plots and to assess pain detection accuracy. As a control, a non-noxious stimulus (6g vF in naive rats and 0.4g vF in CFA- or SNI-treated rats) was delivered to the plantar surface of the hind paw contralateral to the brain recording site in free-moving rats. Non-noxious stimulations were applied for approximately 5 s or until paw withdrawal.

Author Manuscript Author Manuscript Author Manuscript Author Manuscript

Mechanical allodynia test.

A Dixon up-down method with vF filaments was used to measure mechanical allodynia[99]. Prior to testing, the rats were placed in a plexiglass container over a mesh table and acclimated for 20 minutes. A set with logarithmically incremental stiffness (0.45, 0.75, 1.20, 2.55, 4.40, 6.10, 10.50, 15.10) were applied to the hind paw in order to calculate 50% withdrawal thresholds.

For BMI experiments, CFA or SNI-treated rats with optic fiber and electrode implants were placed in a plexiglass chamber over a mesh table and allowed to habituate. 1-5 trials of 6g vF stimulus delivered to the hind paw of the rat were used to train the SSM. Subsequently the rats were allowed a period of rest to avoid hypersensitivity. The testing trials followed the Dixon up-down method. Trials with detection were used to calculate 50% withdrawal thresholds. All stimulations were applied to the plantar surface of the hind paw contralateral to the brain recording site.

Conditioned place aversion test for evoked pain.

CPA experiments were conducted in a connected two-chamber device. Animal movements in each chamber were recorded by a high-speed camera from above the chamber and analyzed with the AnyMaze software (Stoelting Co.), followed by visual verification of the recorded videos by an independent experimenter. The CPA protocol consists of preconditioning (baseline), conditioning, and testing phases. During 10-min preconditioning, the rat was allowed to move freely between the two chambers, and the time spent in each chamber was recorded. Rats that spent more than 500 s or less than 100 s in each chamber during the preconditioning phase were not used in further testing. After the training of the model, the rat was then conditioned with either BMI or random optogenetic activation of the PFC. One of the chambers was paired with BMI and the other chamber with random optogenetic activation of matching intensity, number and duration (control). The animal was confined to one of the associated chambers during each conditioning phase. During conditioning with BMI, the total number and duration of optogenetic activation events were calculated. The same number and duration of optogenetic activation was randomly delivered in the opposite control chamber. Optogenetic activation and chamber pairings were counterbalanced. The same peripheral stimulus was used in both chambers during the conditioning. PP and 6g vF (control) were used for the testing of naïve rats. For experiments with CFA- and SNI-treated rats, 6g vF and 0.4g vF (control) were used to deliver peripheral stimulus to the hind paw, whereas 6g stimulus was used to train the model. During the test phase, the animal was not given any peripheral stimulus or optogenetic activation and had access to move freely between the chambers. The time spent in each chamber was recorded and analyzed.

Conditioned place aversion test for spontaneous or tonic pain.

CPA experiments were conducted for CFA- or SNI-treated rats in a connected two-chamber device. Animal movements in each chamber were recorded by a high-speed camera from above the chamber and analyzed with the AnyMaze software, followed by visual verification of the recorded videos by an independent experimenter. The CPA protocol consists of preconditioning (baseline), conditioning, and testing phases. During the 10 min

Author Manuscript Author Manuscript Author Manuscript Author Manuscript

of preconditioning, the rat was allowed to move freely between the two chambers, and the time spent in each chamber was recorded. Rats that spent more than 500 s or less than 100 s in each chamber during the preconditioning phase were not used in further analysis. Following preconditioning, the SSM was trained with 6g vF filament stimulation of the hind paw. During conditioning (60 min total), no peripheral stimulus was given, but rats received either BMI-triggered optogenetic activation of the prelimbic PFC or random PFC (control) activations of matching duration and intensity. The animal was confined to one of the associated chambers during each conditioning phase. During conditioning with BMI, the total number and duration of optogenetic activation events were calculated, and the same number and duration of activation was randomly delivered in the opposite control chamber. Furthermore, optogenetic activation and chamber pairings were counterbalanced. During the test phase, the animal was not given any peripheral stimulus or optogenetic activation and had access to move freely between the chambers. The time spent in each chamber was recorded and analyzed.

A total of 30 rats were used for all experiments. A subset of rats underwent acute pain assays including the Hargreaves test and CPA for evoked pain prior to chronic pain experiments. These rats were allowed sufficient time (1 week) to recover after acute pain assays and rest, before the onset of chronic pain experiments.

Immunohistochemistry.

Rats were deeply anesthetized with isoflurane and transcardially perfused with ice-cold phosphate-buffered saline (PBS) and paraformaldehyde (PFA). After extraction, brains were fixed in 4% PFA overnight and then transferred to 30% sucrose in PBS to be cryoprotected for 3 days[66]. Next, 20 μm coronal sections were collected using Leica CM3050S cryostat (Leica Biosystems), washed in PBS, and coverslipped with Vectashield mounting medium. Sections from brains containing electrodes were stained with cresyl violet and imaged at 10x magnification with an Axio Zoom widefield microscope (Carl Zeiss). Sections also were made after viral transfer for opsin verification, and these sections were stained with anti-rabbit GFP (1:500, #AB290, Abcam), CaMKII-a (6G9) mouse monoclonal antibody (mAb) (1:200, #50049, Cell Signaling Technology) antibodies, and coverslipped with DAPI (1:200, Vector Laboratories). Secondary antibodies were anti-rabbit immunoglobulin G (IgG) conjugated to Alexa Fluor 488, and anti-mouse IgG conjugated to Alexa Fluor 647 (1:200, Life Technologies). Images were acquired with a Zeiss LSM 700 confocal microscope (Carl Zeiss).

Statistics and Reproducibility.

The neural data and behavior data were offline analyzed by custom MATLAB (Version 2018, MathWorks) scripts, NeuroExplorer (Version 5.0, NeuroExplorer) and GraphPad Prism Version 8 software (GraphPad). Online-sorted spikes were further offline spike sorted by Offline Sorter (4.0, Plexon). For each sorted neuron, a peri-stimulation time histograms (PSTH) was generated 5 s before and after the onset of the peripheral stimulus with 100 ms bin size. The normalized Z-score firing rates at each bin was calculated by the following equation: $Z = (FR - \text{mean of } FR_b) / \text{standard deviation of } FR_b$, where FR indicates firing rate and FR_b indicates baseline firing rate prior to stimulus. A positive or negative response

Author Manuscript Author Manuscript Author Manuscript Author Manuscript

unit was defined by at least 2 consecutive bins firing rates were higher or lower than mean of FR_b+/−3 standard deviation of FR_b within the range (0-5 s) for Hargreaves Test or (0-1 s) for PP and vF test. The cumulative firing rate was calculated by MATLAB function *trapz*. Positive pain onset detection trials were defined by SSM prediction within 5 seconds after stimulus (0-5 s). Detection rates were calculated by positive pain onset detection trials divided by total stimulus trials. When the data normality holds, Student's t test was used to compare Z-scored firing rates across different conditions, and paired t test was used for repeated data. Fisher's exact test was used to analyze the population changes for pain response. When the normality does not hold, we used the nonparametric rank-sum test or signed-rank test.

The results of behavioral experiments were given as mean ± s.e.m. For mechanical allodynia, a one way ANOVA with repeated measures and post-hoc multiple pair-wise comparison Bonferroni tests was used to compute the 50% withdrawal threshold over time, whereas an unpaired Student's t test was used to calculate the difference in allodynia between BMI and control conditions. During the CPA test, a Wilcoxon signed-rank test was used to compare the time spent in each treatment chamber before and after conditioning (i.e. preconditioning vs testing phase for each chamber). A CPA score was calculated by subtracting the time spent in the more noxious chamber during the testing phase from the time spent in that chamber during the preconditioning phase. A two-tailed unpaired Student's t test was used to compare differences in CPA scores under various testing conditions. Experimenter and data analysts were blinded to the condition of rats.

After experiments, animals were sacrificed, and 20 μm brain sections were collected using a Leica CM3050S cryostat machine and analyzed for viral expression, optic fiber localization, and electrode localization with histological staining (Supplementary Fig. 1a, b) to verify fiber or electrode placements and viral expression in the target brain regions. Animals with improper fiber or electrode placements, low viral expression, or viral expression outside the target brain areas were excluded from further analysis.

Reporting summary.

Further information on research design is available in the Nature Research Reporting Summary linked to this article.

Supplementary Material

Refer to Web version on PubMed Central for supplementary material.

Acknowledgements

This work was supported by NIH grants R01-GM115384 (J.W.), R01-NS100065 (Z.S.C., J.W.), and R01-MH118928 (Z.S.C.), and NSF grant CBET-1835000 (Z.S.C., J.W.).

Data availability

The main data supporting the results in this study are available within the paper and its Supplementary Information. The raw datasets generated during the study are too large to be

Author Manuscript Author Manuscript Author Manuscript Author Manuscript

publicly shared, yet they are available for research purposes from the corresponding authors on reasonable request.

References

1. Basbaum AI, Bautista DM, Scherrer G & Julius D Cellular and molecular mechanisms of pain. Cell 139, 267–284 (2009). [PubMed: 19837031]
2. Busse JW, et al. Opioids for Chronic Noncancer Pain: A Systematic Review and Meta-analysis. Jama 320, 2448–2460 (2018). [PubMed: 30561481]
3. Finnerup NB, et al. Pharmacotherapy for neuropathic pain in adults: a systematic review and meta-analysis. The Lancet. Neurology 14, 162–173 (2015). [PubMed: 25575710]
4. Deer TR, et al. The appropriate use of neurostimulation: stimulation of the intracranial and extracranial space and head for chronic pain. Neuromodulation Appropriateness Consensus Committee. Neuromodulation 17, 551–570; discussion 570 (2014). [PubMed: 25112890]
5. Coffey RJ Deep brain stimulation for chronic pain: results of two multicenter trials and a structured review. Pain Med 2, 183–192 (2001). [PubMed: 15102250]
6. Nandi D, Aziz T, Carter H & Stein J Thalamic field potentials in chronic central pain treated by periventricular gray stimulation -- a series of eight cases. Pain 101, 97–107 (2003). [PubMed: 12507704]
7. Owen SL, et al. Deep brain stimulation for neuropathic pain. Acta Neurochir Suppl 97, 111–116 (2007).
8. Green AL, et al. N-of-1 Trials for Assessing the Efficacy of Deep Brain Stimulation in Neuropathic Pain. Neuromodulation 7, 76–81 (2004). [PubMed: 22151187]
9. Bittar RG, et al. Deep brain stimulation for pain relief: a meta-analysis. J Clin Neurosci 12, 515–519 (2005). [PubMed: 15993077]
10. Boccard SG, Pereira EA, Moir L, Aziz TZ & Green AL Long-term outcomes of deep brain stimulation for neuropathic pain. Neurosurgery 72, 221–230; discussion 231 (2013). [PubMed: 23149975]
11. Marchand S, Kupers RC, Bushnell MC & Duncan GH Analgesic and placebo effects of thalamic stimulation. Pain 105, 481–488 (2003). [PubMed: 14527708]
12. Spooner J, Yu H, Kao C, Sillay K & Konrad P Neuromodulation of the cingulum for neuropathic pain after spinal cord injury. Case report. J Neurosurg 107, 169–172 (2007). [PubMed: 17639889]
13. Boccard SG, et al. Deep brain stimulation of the anterior cingulate cortex: targeting the affective component of chronic pain. Neuroreport 25, 83–88 (2014). [PubMed: 24100411]
14. Lende RA, Kirsch WM & Druckman R Relief of facial pain after combined removal of precentral and postcentral cortex. J Neurosurg 34, 537–543 (1971). [PubMed: 5554359]
15. Tsubokawa T, Katayama Y, Yamamoto T, Hirayama T & Koyama S Chronic motor cortex stimulation for the treatment of central pain. Acta Neurochir Suppl (Wien) 52, 137–139 (1991). [PubMed: 1792954]
16. Katayama Y, Tsubokawa T & Yamamoto T Chronic motor cortex stimulation for central deafferentation pain: experience with bulbar pain secondary to Wallenberg syndrome. Stereotact Funct Neurosurg 62, 295–299 (1994). [PubMed: 7631085]
17. Katayama Y, Fukaya C & Yamamoto T Poststroke pain control by chronic motor cortex stimulation: neurological characteristics predicting a favorable response. J Neurosurg 89, 585–591 (1998). [PubMed: 9761052]
18. Herregodts P, Stadnik T, De Ridder F & D'Haens J Cortical stimulation for central neuropathic pain: 3-D surface MRI for easy determination of the motor cortex. Acta Neurochir Suppl 64, 132–135 (1995). [PubMed: 8748601]
19. Ebel H, Rust D, Tronnier V, Boker D & Kunze S Chronic precentral stimulation in trigeminal neuropathic pain. Acta Neurochir (Wien) 138, 1300–1306 (1996). [PubMed: 8980733]
20. Nguyen JP, et al. [Treatment of central and neuropathic facial pain by chronic stimulation of the motor cortex: value of neuronavigation guidance systems for the localization of the motor cortex]. Neurochirurgie 46, 483–491 (2000). [PubMed: 11084480]

Author Manuscript Author Manuscript Author Manuscript Author Manuscript

21. Garcia-Larrea L, et al. Electrical stimulation of motor cortex for pain control: a combined PET-scan and electrophysiological study. Pain 83, 259–273 (1999). [PubMed: 10534598]
22. Lenz FA, Kwan HC, Dostrovsky JO & Tasker RR Characteristics of the bursting pattern of action potentials that occurs in the thalamus of patients with central pain. Brain Res 496, 357–360 (1989). [PubMed: 2804648]
23. Tasker RR, Gorecki J, Lenz FA, Hirayama T & Dostrovsky JO Thalamic microelectrode recording and microstimulation in central and deafferentation pain. Appl Neurophysiol 50, 414–417 (1987). [PubMed: 3329877]
24. Lenz FA, et al. Abnormal single-unit activity recorded in the somatosensory thalamus of a quadriplegic patient with central pain. Pain 31, 225–236 (1987). [PubMed: 3501563]
25. Mazars G, Merienne L & Cioloca C [Treatment of certain types of pain with implantable thalamic stimulators]. Neurochirurgie 20, 117–124 (1974). [PubMed: 4418054]
26. Mazars G, Merienne L & Ciolocca C [Intermittent analgesic thalamic stimulation. Preliminary note]. Rev Neurol (Paris) 128, 273–279 (1973). [PubMed: 4774913]
27. Turnbull IM, Shulman R & Woodhurst WB Thalamic stimulation for neuropathic pain. J Neurosurg 52, 486–493 (1980). [PubMed: 6966326]
28. Richardson DE & Akil H Pain reduction by electrical brain stimulation in man. Part 1: Acute administration in periaqueductal and periventricular sites. J Neurosurg 47, 178–183 (1977). [PubMed: 327030]
29. Richardson DE & Akil H Pain reduction by electrical brain stimulation in man. Part 2: Chronic self-administration in the periventricular gray matter. J Neurosurg 47, 184–194 (1977). [PubMed: 301558]
30. Hosobuchi Y, Adams JE & Linchitz R Pain relief by electrical stimulation of the central gray matter in humans and its reversal by naloxone. Science 197, 183–186 (1977). [PubMed: 301658]
31. Boccard SG, Pereira EA & Aziz TZ Deep brain stimulation for chronic pain. Journal of clinical neuroscience : official journal of the Neurosurgical Society of Australasia 22, 1537–1543 (2015). [PubMed: 26122383]
32. Sadtler PT, et al. Neural constraints on learning. Nature 512, 423–426 (2014). [PubMed: 25164754]
33. Berenyi A, Belluscio M, Mao D & Buzsaki G Closed-loop control of epilepsy by transcranial electrical stimulation. Science 337, 735–737 (2012). [PubMed: 22879515]
34. Bergey GK, et al. Long-term treatment with responsive brain stimulation in adults with refractory partial seizures. Neurology 84, 810–817 (2015). [PubMed: 25616485]
35. Heck CN, et al. Two-year seizure reduction in adults with medically intractable partial onset epilepsy treated with responsive neurostimulation: final results of the RNS System Pivotal trial. Epilepsia 55, 432–441 (2014). [PubMed: 24621228]
36. Morrell MJ & Group, R.N.S.S.i.E.S. Responsive cortical stimulation for the treatment of medically intractable partial epilepsy. Neurology 77, 1295–1304 (2011). [PubMed: 21917777]
37. Ajiboye AB, et al. Restoration of reaching and grasping movements through brain-controlled muscle stimulation in a person with tetraplegia: a proof-of-concept demonstration. Lancet 389, 1821–1830 (2017). [PubMed: 28363483]
38. Taylor DM, Tillery SI & Schwartz AB Direct cortical control of 3D neuroprosthetic devices. Science 296, 1829–1832 (2002). [PubMed: 12052948]
39. Hochberg LR, et al. Neuronal ensemble control of prosthetic devices by a human with tetraplegia. Nature 442, 164–171 (2006). [PubMed: 16838014]
40. Hochberg LR, et al. Reach and grasp by people with tetraplegia using a neurally controlled robotic arm. Nature 485, 372–375 (2012). [PubMed: 22596161]
41. Collinger JL, et al. High-performance neuroprosthetic control by an individual with tetraplegia. Lancet 381, 557–564 (2013). [PubMed: 23253623]
42. Aflalo T, et al. Neurophysiology. Decoding motor imagery from the posterior parietal cortex of a tetraplegic human. Science 348, 906–910 (2015). [PubMed: 25999506]
43. Wenger N, et al. Closed-loop neuromodulation of spinal sensorimotor circuits controls refined locomotion after complete spinal cord injury. Sci Transl Med 6, 255ra133 (2014).

Author Manuscript Author Manuscript Author Manuscript Author Manuscript

44. Wagner FB, et al. Targeted neurotechnology restores walking in humans with spinal cord injury. Nature 563, 65–71 (2018). [PubMed: 30382197]
45. Anumanchipalli GK, Chartier J & Chang EF Speech synthesis from neural decoding of spoken sentences. Nature 568, 493–498 (2019). [PubMed: 31019317]
46. Shanechi MM Brain-machine interfaces from motor to mood. Nature neuroscience 22, 1554–1564 (2019). [PubMed: 31551595]
47. Grosenick L, Marshel JH & Deisseroth K Closed-loop and activity-guided optogenetic control. Neuron 86, 106–139 (2015). [PubMed: 25856490]
48. Mickle AD, et al. A wireless closed-loop system for optogenetic peripheral neuromodulation. Nature 565, 361–365 (2019). [PubMed: 30602791]
49. Turnbull IM Bilateral cingulumotomy combined with thalamotomy or mesencephalic tractotomy for pain. Surg Gynecol Obstet 134, 958–962 (1972). [PubMed: 4113363]
50. Rainville P, Duncan GH, Price DD, Carrier B & Bushnell MC Pain affect encoded in human anterior cingulate but not somatosensory cortex. Science 277, 968–971 (1997). [PubMed: 9252330]
51. Foltz EL & White LE The role of rostral cingulumotomy in “pain” relief. Int J Neurol 6, 353–373 (1968). [PubMed: 5759640]
52. Qu C, et al. Lesion of the rostral anterior cingulate cortex eliminates the aversiveness of spontaneous neuropathic pain following partial or complete axotomy. Pain 152, 1641–1648 (2011). [PubMed: 21474245]
53. Johansen JP, Fields HL & Manning BH The affective component of pain in rodents: direct evidence for a contribution of the anterior cingulate cortex. Proc Natl Acad Sci U S A 98, 8077–8082 (2001). [PubMed: 11416168]
54. LaGraize SC, Borzan J, Peng YB & Fuchs PN Selective regulation of pain affect following activation of the opioid anterior cingulate cortex system. Exp Neurol 197, 22–30 (2006). [PubMed: 15996657]
55. Lubar JF Effect of Medial Cortical Lesions on the Avoidance Behavior of the Cat. J Comp Physiol Psychol 58, 38–46 (1964). [PubMed: 14197039]
56. Melzack R.a.C., L. K Sensory, motivational, and central control determinants of pain: a new conceptual model. The Skin Senses., 423–443 (1968).
57. Chen Z, Zhang Q, Tong AP, Manders TR & Wang J Deciphering neuronal population codes for acute thermal pain. J Neural Eng 14, 036023 (2017). [PubMed: 28384122]
58. Hu S, Zhang Q, Wang J & Chen Z Real-time particle filtering and smoothing algorithms for detecting abrupt changes in neural ensemble spike activity. J Neurophysiol 119, 1394–1410 (2018). [PubMed: 29357468]
59. Zhang Q, et al. Chronic pain induces generalized enhancement of aversion. Elife 6(2017).
60. Lewin W & Whitty CW Effects of anterior cingulate stimulation in conscious human subjects. J Neurophysiol 23, 445–447 (1960). [PubMed: 14416482]
61. Buchel C, et al. Dissociable neural responses related to pain intensity, stimulus intensity, and stimulus awareness within the anterior cingulate cortex: a parametric single-trial laser functional magnetic resonance imaging study. J Neurosci 22, 970–976 (2002). [PubMed: 11826125]
62. Meda KS, et al. Microcircuit Mechanisms through which Mediodorsal Thalamic Input to Anterior Cingulate Cortex Exacerbates Pain-Related Aversion. Neuron 102, 944–959 e943 (2019). [PubMed: 31030955]
63. Hutchison WD, Davis KD, Lozano AM, Tasker RR & Dostrovsky JO Pain-related neurons in the human cingulate cortex. Nat Neurosci 2, 403–405 (1999). [PubMed: 10321241]
64. Sikes RW & Vogt BA Nociceptive neurons in area 24 of rabbit cingulate cortex. J Neurophysiol 68, 1720–1732 (1992). [PubMed: 1479441]
65. Li XY, et al. Alleviating neuropathic pain hypersensitivity by inhibiting PKMzeta in the anterior cingulate cortex. Science 330, 1400–1404 (2010). [PubMed: 21127255]
66. Singh A, et al. Mapping Cortical Integration of Sensory and Affective Pain Pathways. Curr Biol 30, 1703–1715 e1705 (2020). [PubMed: 32220320]

Author Manuscript Author Manuscript Author Manuscript Author Manuscript

67. Lee M, et al. Activation of corticostriatal circuitry relieves chronic neuropathic pain. J Neurosci 35, 5247–5259 (2015). [PubMed: 25834050]
68. Martinez E, et al. Corticostriatal Regulation of Acute Pain. Front Cell Neurosci 11, 146 (2017). [PubMed: 28603489]
69. Zhang Z, et al. Role of Prelimbic GABAergic Circuits in Sensory and Emotional Aspects of Neuropathic Pain. Cell Rep 12, 752–759 (2015). [PubMed: 26212331]
70. Hardy SG Analgesia elicited by prefrontal stimulation. Brain Res 339, 281–284 (1985). [PubMed: 4027626]
71. Kiritoshi T, Ji G & Neugebauer V Rescue of Impaired mGluR5-Driven Endocannabinoid Signaling Restores Prefrontal Cortical Output to Inhibit Pain in Arthritic Rats. J Neurosci 36, 837–850 (2016). [PubMed: 26791214]
72. Dale J, et al. Scaling Up Cortical Control Inhibits Pain. Cell Rep 23, 1301–1313 (2018). [PubMed: 29719246]
73. Ji G, et al. Cognitive impairment in pain through amygdala-driven prefrontal cortical deactivation. J Neurosci 30, 5451–5464 (2010). [PubMed: 20392966]
74. Huang J, et al. A neuronal circuit for activating descending modulation of neuropathic pain. Nat Neurosci 22, 1659–1668 (2019). [PubMed: 31501573]
75. Cheriyan J & Sheets PL Altered Excitability and Local Connectivity of mPFC-PAG Neurons in a Mouse Model of Neuropathic Pain. J Neurosci 38, 4829–4839 (2018). [PubMed: 29695413]
76. Metz AE, Yau HJ, Centeno MV, Apkarian AV & Martina M Morphological and functional reorganization of rat medial prefrontal cortex in neuropathic pain. Proc Natl Acad Sci U S A 106, 2423–2428 (2009). [PubMed: 19171885]
77. Vertes RP Interactions among the medial prefrontal cortex, hippocampus and midline thalamus in emotional and cognitive processing in the rat. Neuroscience 142, 1–20 (2006). [PubMed: 16887277]
78. Apkarian AV, et al. Chronic back pain is associated with decreased prefrontal and thalamic gray matter density. J Neurosci 24, 10410–10415 (2004). [PubMed: 15548656]
79. Zhou H, et al. Ketamine reduces aversion in rodent pain models by suppressing hyperactivity of the anterior cingulate cortex. Nat Commun 9, 3751 (2018). [PubMed: 30218052]
80. King T, et al. Unmasking the tonic-aversive state in neuropathic pain. Nat Neurosci 12, 1364–1366 (2009). [PubMed: 19783992]
81. Decosterd I & Woolf CJ Spared nerve injury: an animal model of persistent peripheral neuropathic pain. Pain 87, 149–158 (2000). [PubMed: 10924808]
82. De Felice M, et al. Capturing the aversive state of cephalic pain preclinically. Ann Neurol (2013).
83. Navratilova E, et al. Endogenous opioid activity in the anterior cingulate cortex is required for relief of pain. J Neurosci 35, 7264–7271 (2015). [PubMed: 25948274]
84. Johansen JP & Fields HL Glutamatergic activation of anterior cingulate cortex produces an aversive teaching signal. Nat Neurosci 7, 398–403 (2004). [PubMed: 15004562]
85. Xiao Z, et al. Cortical Pain Processing in the Rat Anterior Cingulate Cortex and Primary Somatosensory Cortex. Front Cell Neurosci 13, 165 (2019). [PubMed: 31105532]
86. Karim F, Wang CC & Gereau R.W.t. Metabotropic glutamate receptor subtypes 1 and 5 are activators of extracellular signal-regulated kinase signaling required for inflammatory pain in mice. J Neurosci 21, 3771–3779 (2001). [PubMed: 11356865]
87. Hu HJ, Alter BJ, Carrasquillo Y, Qiu CS & Gereau R.W.t. Metabotropic glutamate receptor 5 modulates nociceptive plasticity via extracellular signal-regulated kinase-Kv4.2 signaling in spinal cord dorsal horn neurons. J Neurosci 27, 13181–13191 (2007). [PubMed: 18045912]
88. O'Callaghan JP & Holtzman SG Quantification of the analgesic activity of narcotic antagonists by a modified hot-plate procedure. J Pharmacol Exp Ther 192, 497–505 (1975). [PubMed: 1168252]
89. Cheppudira BP Characterization of hind paw licking and lifting to noxious radiant heat in the rat with and without chronic inflammation. J Neurosci Methods 155, 122–125 (2006). [PubMed: 16574243]
90. Kang SJ, et al. Bidirectional modulation of hyperalgesia via the specific control of excitatory and inhibitory neuronal activity in the ACC. Mol Brain 8, 81 (2015). [PubMed: 26631249]

Author Manuscript Author Manuscript Author Manuscript Author Manuscript

91. Langford DJ, et al. Coding of facial expressions of pain in the laboratory mouse. Nat Methods 7, 447–449 (2010). [PubMed: 20453868]
92. Tappe-Theodor A & Kuner R Studying ongoing and spontaneous pain in rodents--challenges and opportunities. Eur J Neurosci 39, 1881–1890 (2014). [PubMed: 24888508]
93. Beric A, et al. Complications of deep brain stimulation surgery. Stereotact Funct Neurosurg 77, 73–78 (2001). [PubMed: 12378060]
94. Alomar S, et al. Speech and language adverse effects after thalamotomy and deep brain stimulation in patients with movement disorders: A meta-analysis. Mov Disord 32, 53–63 (2017). [PubMed: 28124434]
95. Xiao Z, et al. Ensembles of change-point detectors: implications for real-time BMI applications. J Comput Neurosci 46, 107–124 (2019). [PubMed: 30206733]
96. Chen Z Advanced state space methods for neural and clinical data., (Cambridge University Press, 2015).
97. Eden UT, Frank LM, Barbieri R, Solo V & Brown EN Dynamic analysis of neural encoding by point process adaptive filtering. Neural Comput 16, 971–998 (2004). [PubMed: 15070506]
98. Hu S ZQ, Wang J, Chen Z . A real-time rodent neural interface for deciphering acute pain signals from neuronal ensemble spike activity. Proc. Asilomar Conf. Signals, Systems & Computers, 93–97 (2017).
99. Wang J, et al. A single subanesthetic dose of ketamine relieves depression-like behaviors induced by neuropathic pain in rats. Anesthesiology 115, 812–821 (2011). [PubMed: 21934410]

Author Manuscript Author Manuscript Author Manuscript Author Manuscript

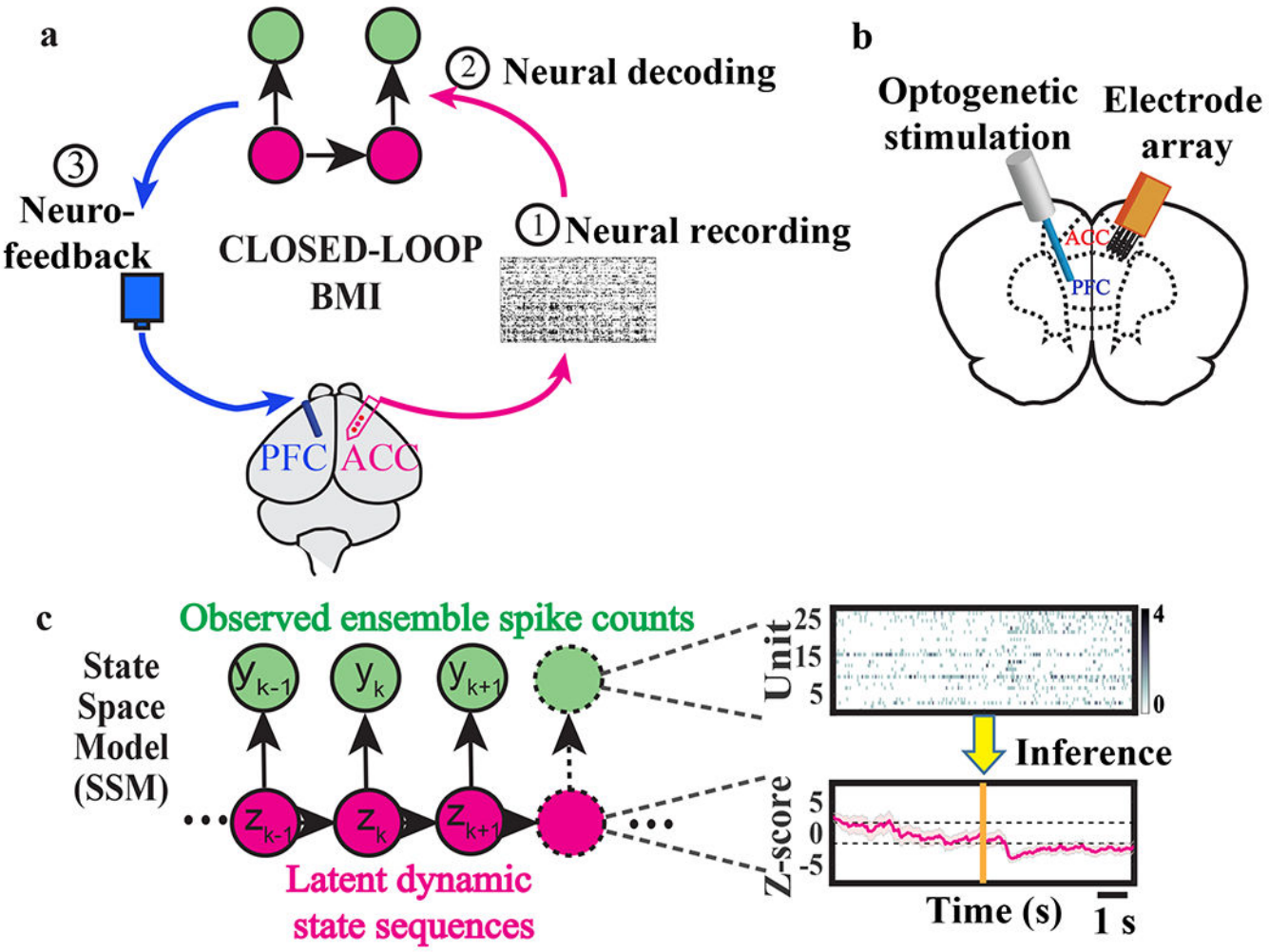

Fig. 1 |. Design of a closed-loop brain-machine interface (BMI) to detect and treat pain.

a, Schematic of BMI that consists of three steps: (1) Neural recording and online signal processing including spike sorting; (2) neural decoding for pain onset detection based on sorted units; (3) pain onset detection to trigger therapeutic neurostimulation as neurofeedback. The magenta and green circular symbols with black arrows indicate the state-space model (SSM, details below). The curved magenta arrows denote data flow for the model inputs, while the curved blue arrows denote the model outputs for therapeutic neurostimulation. The blue box denotes the laser. **b,** Placement of optic fiber in the prelimbic prefrontal cortex (PFC) and recording electrodes in the anterior cingulate cortex (ACC). **c,** Left: schematic of the state-space model (SSM) for detecting the change point (pain onset) from the neuronal ensemble spike activity. Right: an example of pain onset detection using the SSM-based decoding strategy. The top example raster plot shows online sorted population spike counts (bin size = 50 ms), with the darker color representing greater spike counts. The unit of color bar is spikes/bin. The bottom magenta trace represents the estimated Z-score from the univariate latent state, and the shaded area marks the 95% confidence intervals (CI). Horizontal dashed lines mark the significance thresholds. Vertical yellow line denotes the onset of noxious stimulation. In the training phase, the SSM

Author Manuscript Author Manuscript Author Manuscript Author Manuscript

parameters were inferred from the ACC ensemble spike data as represented by the top raster plot. In the testing phase, a one-dimensional discrete-time latent dynamic state sequence $\{z_k\}$ (k=1,…,T) was inferred from the SSM, and the bottom Z-score (magenta trace) was calculated from the inferred latent state variable (see Methods).

Author Manuscript Author Manuscript Author Manuscript Author Manuscript

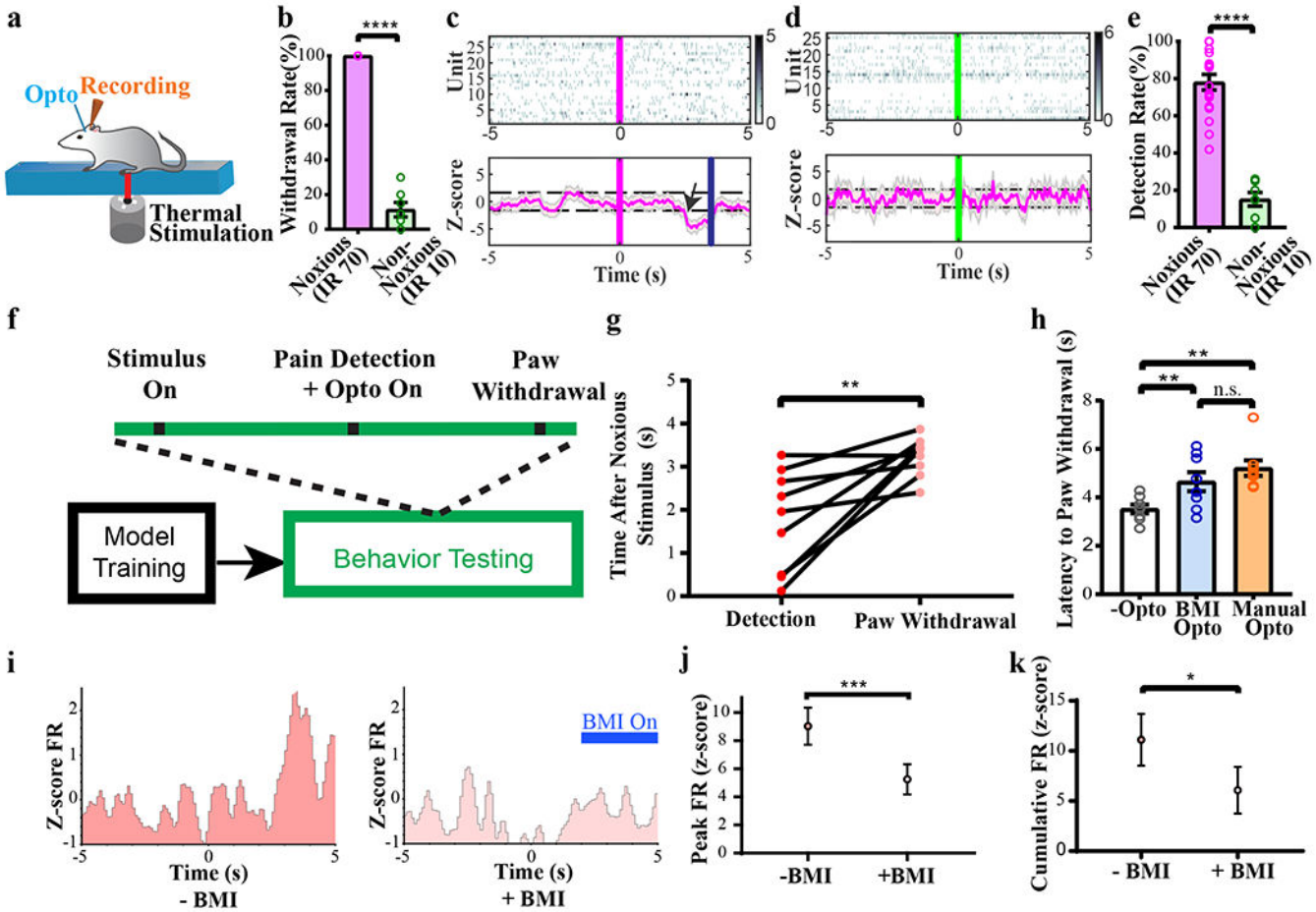

Fig. 2 |. Closed-loop BMI control of acute thermal pain.

a, Schematic of BMI experiments during thermal pain delivery with an infrared (IR) emitter. Stimulus presentation lasted until paw withdrawal or 5 s. **b,** Peripheral nocifensive behavioral response to thermal stimulation. A noxious stimulus (IR 70) triggered paw withdrawals, whereas a non-noxious stimulus (IR 10) did not. Withdrawal rate, defined as the percentage of peripheral stimulations that resulted in observed paw withdrawal, is shown. n = 7 rats used with non-noxious stimulation (IR 10), n = 17 rats used with noxious stimulation (IR 70); $p < 0.0001$, two-sided unpaired Student's t test. Data are presented as mean ± s.e.m. of biological replicates. **c, d,** Example SSM detection performances. The SSM-based decoder detected the onset of an pain episode in a single trial in response to noxious stimulation (**c**), in contrast to a trial with non-noxious stimulation (**d**). The top raster plots show online sorted population spike counts (bin size =50 ms), with the darker color representing greater spike counts. The unit of color bar is spikes/bin. The bottom magenta trace represents the estimated Z-score from the univariate latent state, and the shaded area marks the 95% confidence intervals (CI). Horizontal dashed lines mark the significance thresholds (see Methods). The vertical magenta and green lines indicate the time of peripheral stimulation; magenta: noxious stimulus; green: non-noxious stimulus. The vertical blue line indicates the time of paw withdrawal. The black arrow indicates the decoded pain onset. n=28 biologically independent neurons recorded in the example session

Author Manuscript Author Manuscript Author Manuscript Author Manuscript

(panel **c**), and n=26 biologically independent neurons in the example session (panel **d**). **e,** The performance of SSM-based decoder in detecting thermal pain. Pain detection rates were calculated as a percentage of trials that had positive pain onset detection. n = 7 rats used with non-noxious stimulation (IR 10), n = 18 rats used with noxious stimulation (IR 70); $p < 0.0001$, two-sided unpaired Student's t test. Data are presented as mean ± s.e.m. of biological replicates. **f,** Schematic of SSM-decoder training and behavior testing with BMI. **g,** Pain onset detection occurred prior to withdrawal responses to noxious thermal stimulations. n = 9 sessions from 6 biologically independent rats; $p = 0.0057$, two-sided paired Student's t test. **h,** Application of the closed-loop BMI prolonged the withdrawal latency on Hargreaves test. n = 8 rats. No opto vs. BMI opto: $p = 0.0074$, no opto vs. manual opto: $p = 0.0027$, BMI opto vs. manual opto: $p = 0.4486$, one-way ANOVA, two-sided Tukey's multiple comparisons test with repeated measures. Data are presented as mean ± s.e.m. of biological replicates. **i,** Left: a representative ACC neuron increased firing rates in response to a noxious thermal stimulus (IR 70). Right: BMI reduced firing rate changes in response to the noxious stimulus. Time 0 indicates the onset of the stimulus. FR: firing rates. **j,** BMI treatment reduced the peak firing rates of pain-responsive ACC neurons in response to the noxious stimulus (see Methods). n = 33 neurons from 6 rats, $p = 0.0001$, two-sided paired Student's t test. Data are presented as mean ± s.e.m. of biological replicates. **k**, BMI treatment reduced cumulative firing rate response of ACC neurons over a 5-s period (within the [0, 5] s range, where time 0 indicates the onset of the stimulus) in response to the noxious stimulus. n = 33 neurons from 6 rats, $p = 0.0135$, two-sided paired Student's t test. Data are presented as mean ± s.e.m. of biological replicates.

Author Manuscript Author Manuscript Author Manuscript Author Manuscript

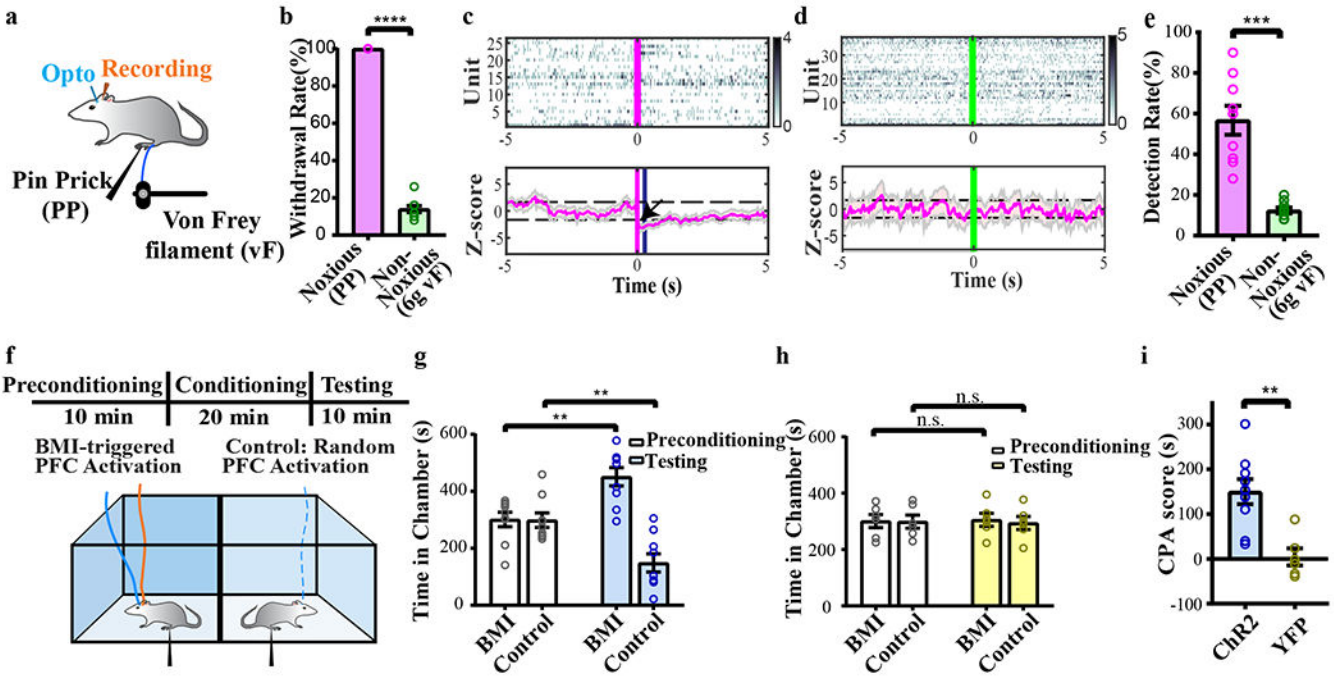

Fig. 3 |. Closed-loop BMI control of acute mechanical pain.

a, Schematic of BMI experiments during mechanical stimulus delivery. **b,** Peripheral nocifensive behavioral response to mechanical stimulation. A noxious stimulus (pin prick or PP) triggered paw withdrawals, whereas a non-noxious stimulus (6g von Frey filament, or vF) did not. Withdrawal rate, defined as the percentage of peripheral stimulations that resulted in observed paw withdrawal, is shown. n = 9 rats; $p < 0.0001$, two-sided paired Student's t test. Data are presented as mean ± s.e.m. of biological replicates. **c, d,** The SSM-based decoder detected the onset of a pain episode in a single trial in response to noxious stimulation (PP, panel **c**), in contrast to a trial with non-noxious stimulation (6g vF, panel **d**). The top raster plots show online sorted population spike counts (bin size =50 ms), with the darker color representing greater spike counts. The unit of color bar is spikes/bin. The bottom magenta trace represents the estimated Z-score from the univariate latent state, and the shaded area marks the 95% confidence intervals (CI). Horizontal dashed lines mark the significance thresholds (see Methods). The vertical magenta and green lines indicate the time of peripheral stimulation. magenta: noxious stimulus; green: non-noxious stimulus. The vertical blue line indicates the time of paw withdrawal. The black arrow indicates the decoded pain onset. n=26 biologically independent neurons in panel **c**, and n=37 neurons in panel **d**. **e,** The performance of SSM-based decoder in detecting mechanical pain. Detection rates were calculated as a percentage of trials that had positive pain onset detection. n = 9 rats; $p = 0.0002$, two-sided paired Student's t test. Data are presented as mean ± s.e.m. of biological replicates. **f,** Schematic of the conditioned place aversion (CPA) assay to assess pain aversion. In a two-chamber set up, aversive response was triggered by a noxious mechanical stimulus (PP) applied to the hind paws. One of the chambers was paired with BMI, and the opposite chamber was paired with random PFC activation of matching duration and intensity. The orange solid line on the rat's head denotes BMI decoding, while the blue line denotes optogenetic stimulation. In the control chamber, the dashed blue line

Author Manuscript Author Manuscript Author Manuscript Author Manuscript

indicates random optogenetic stimulation. **g,** After conditioning, ChR2 rats preferred BMI treatment chamber. n = 9 rats; p = 0.0039, two-sided Wilcoxon signed-rank test. Data are presented as mean ± s.e.m. of biological replicates. **h,** YFP control rats demonstrated no preference for the BMI treatment. n = 6 rats; p = 0.8438, two-sided Wilcoxon signed-rank test. Data are presented as mean ± s.e.m. of biological replicates. **i,** CPA scores for BMI treatment in rats that experienced acute mechanical pain. n = 9 rats with ChR2 injection, n = 6 control rats with YFP injection; p = 0.0016, two-sided Mann-Whitney U test. Data are presented as mean ± s.e.m. of biological replicates.

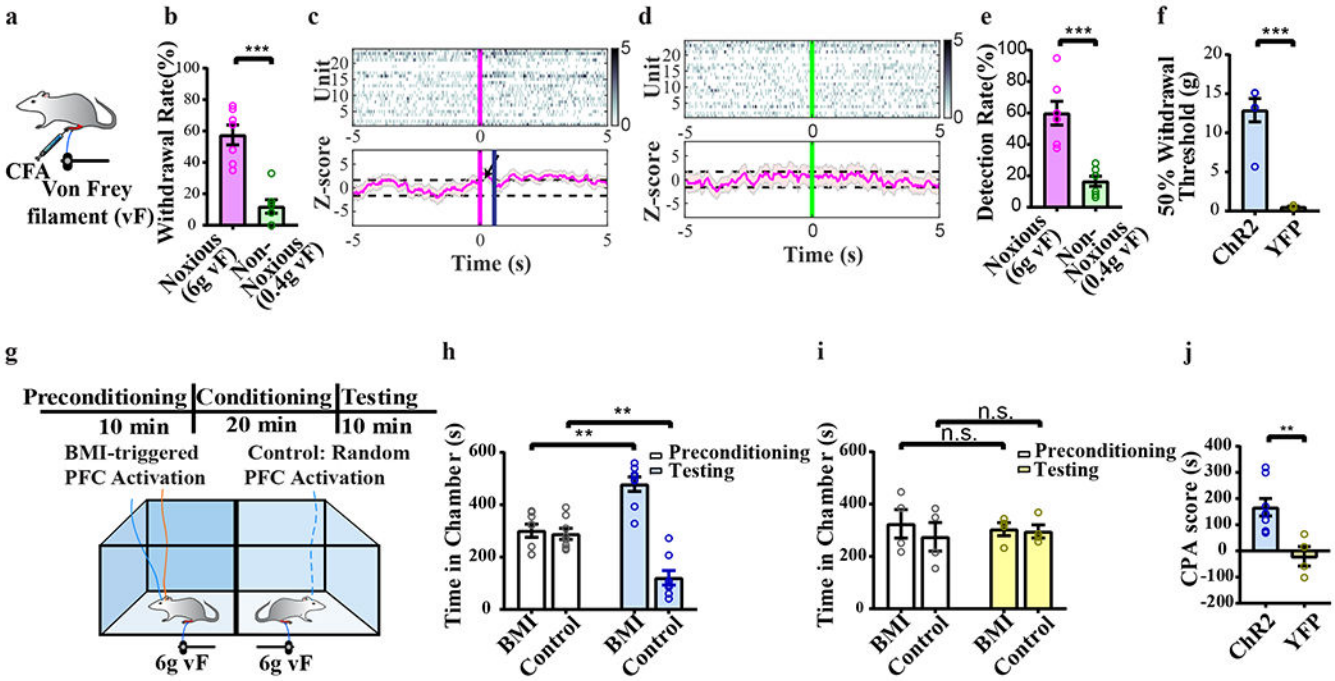

Fig. 4 |. Closed-loop BMI control of evoked pain in a model of chronic inflammatory pain.

a, Schematic for the CFA model of inflammatory pain. **b,** Peripheral allodynia response after CFA treatment. 6g vF triggered paw withdrawals, whereas 0.4g vF did not. Withdrawal rate, defined as the percentage of peripheral stimulations that resulted in observed paw withdrawal, is shown. n = 7 rats; p = 0.0008, two-sided paired Student's t test. Data are presented as mean ± s.e.m of biological replicates. **c, d,** The SSM-based decoder detected the onset of a pain episode in a single trial in response to peripheral allodynia-inducing stimulus (6g vF, panel **c**) in a CFA-treated rat, in contrast to a trial with a non-allodynia-inducing stimulus (0.4g vF, panel **d**). The top raster plots show online sorted population spike counts (bin size =50 ms), with the darker color representing greater spike counts. The unit of color bar is spikes/bin. The bottom magenta trace represents the estimated Z-score from the univariate latent state, and the shaded area marks the 95% confidence intervals (CI). Horizontal dashed lines mark the significance thresholds (see Methods). The vertical magenta and green lines indicate the time of peripheral stimulation. magenta: 6g vF stimulus; green: 0.4g vF stimulus. The vertical blue line indicates the time of paw withdrawal. The black arrow indicates the decoded pain onset. n=24 biologically independent neurons in panel **c**, and n=24 neurons in panel **d**. **e,** The performance of SSM-based decoder in detecting the onset of mechanical allodynia in CFA-treated rats. Detection rates were calculated as a percentage of trials that had positive pain onset detection. n = 7 rats; p = 0.0008, two-sided paired Student's t test. Data are presented as mean ± s.e.m. of biological replicates. **f,** Closed-loop BMI inhibited mechanical allodynia in CFA-treated rats. n = 6 rats with ChR2 injection, n = 4 control rats with YFP injection; p = 0.0002, two-sided unpaired Student's t test. Data are presented as mean ± s.e.m. of biological replicates. **g,** Schematic of the conditioned place aversion (CPA) assay in CFA-treated rats. Aversive response was triggered by an allodynia-inducing mechanical stimulus (6g vF) applied in both chambers. One of the chambers was paired with BMI, and the opposite chamber was

Author Manuscript
Author Manuscript
Author Manuscript
Author Manuscript

Author Manuscript Author Manuscript Author Manuscript Author Manuscript

paired with random PFC activation of matching duration and intensity. The orange solid line on the rat's head denotes BMI decoding, while the blue line denotes optogenetic stimulation. In the control chamber, the dashed blue line indicates random optogenetic stimulation. **h,** In ChR2 rats, BMI treatment reduced aversion associated with mechanical allodynia (triggered by the 6g vF stimulus) in the CFA model. n = 8 rats; p = 0.0078, two-sided Wilcoxon signed-rank test. Data are presented as mean ± s.e.m. of biological replicates. **i,** YFP control rats demonstrated no preference for the BMI treatment. n = 4 rats; p = 0.8750, two-sided Wilcoxon signed-rank test. Data are presented as mean ± s.e.m. of biological replicates. **j,** CPA scores for BMI treatment in CFA-treated rats. n = 8 rats with ChR2 injection, n = 4 control rats with YFP injection; p = 0.0040, two-sided Mann-Whitney U test. Data are presented as mean ± s.e.m. of biological replicates.

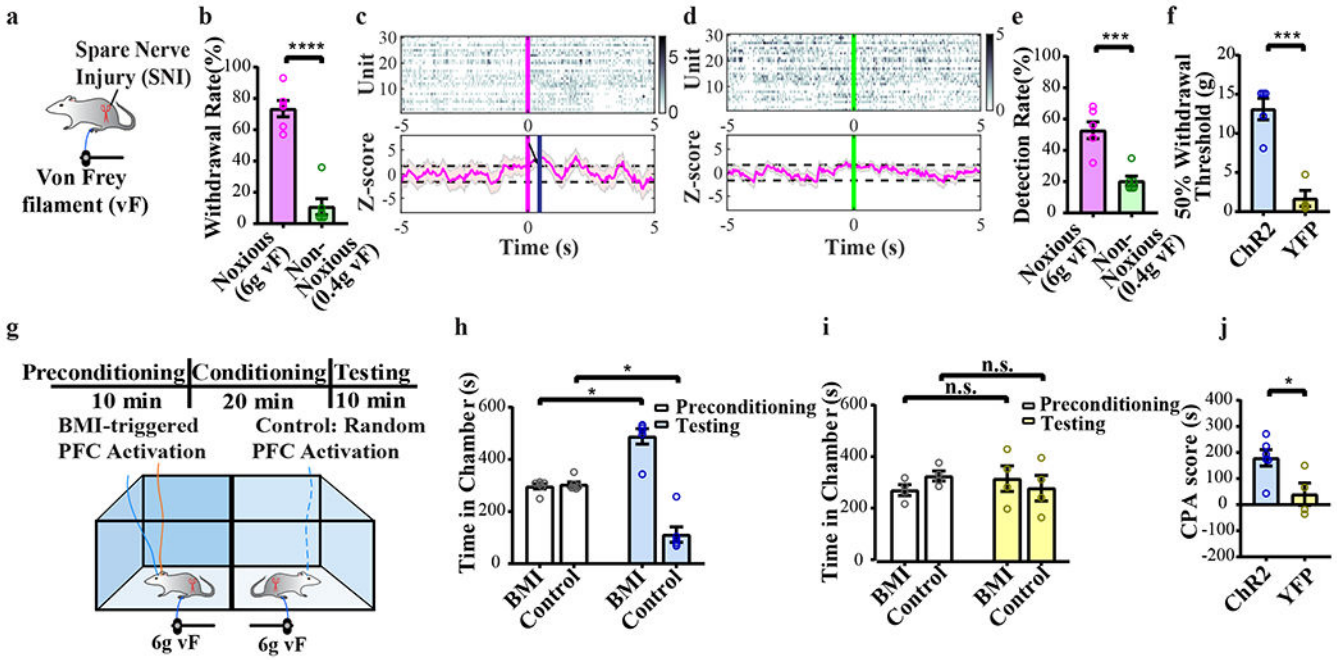

Fig. 5 |. Closed-loop BMI control of evoked pain in a model of chronic neuropathic pain.

a, Schematic for the SNI model of chronic neuropathic pain. **b,** Peripheral allodynia response after SNI. 6g vF triggered paw withdrawals, whereas 0.4g vF did not. Withdrawal rate, defined as the percentage of peripheral stimulations that resulted in observed paw withdrawal, is shown. n = 6 rats; $p < 0.0001$, two-sided paired Student's t test. Data are presented as mean ± s.e.m. of biological replicates. **c, d,** The SSM-based decoder detected the onset of a pain episode in a single trial in response to peripheral allodynia-inducing stimulus (6g vF, panel **c**) in a SNI-treated rat, in contrast to a trial with a non-allodynia-inducing stimulus (0.4g vF, panel **d**). The top raster plots show online sorted population spike counts (bin size =50 ms), with the darker color representing greater spike counts. The unit of color bar is spikes/bin. The bottom magenta trace represents the estimated Z-score from the univariate latent state, and the shaded area marks the 95% confidence intervals (CI). Horizontal dashed lines mark the significance thresholds (see Methods). The vertical magenta and green lines indicate the time of peripheral stimulation. magenta: 6g vF stimulus; green: 0.4g vF stimulus. The vertical blue line indicates the time of paw withdrawal. The black arrow indicates the decoded pain onset. n=30 biologically independent neurons in panel **c**, and n=30 neurons in panel **d**. **e,** The performance of SSM-based decoder in detecting mechanical allodynia in SNI-treated rats. Detection rates were calculated as a percentage of trials that had positive pain onset detection. n = 6 rats; $p = 0.0008$, two-sided paired Student's t test. Data are presented as mean ± s.e.m. of biological replicates. **f,** Closed-loop BMI inhibited mechanical allodynia in the SNI model. n = 5 rats with ChR2 injection, n = 4 control rats with YFP injection; $p = 0.0004$, two-sided unpaired Student's t test. Data are presented as mean ± s.e.m. of biological replicates. **g,** Schematic of the CPA assay in SNI-treated rats. Aversive response was triggered by an allodynia-inducing mechanical stimulus (6g vF) applied in both chambers. One of the chambers was paired with BMI, and the opposite chamber was paired with random PFC activation of matching

Author Manuscript
Author Manuscript
Author Manuscript
Author Manuscript

Author Manuscript

Author Manuscript

Author Manuscript

Author Manuscript

duration and intensity. The orange solid line on the rat's head denotes BMI decoding, while the blue line denotes optogenetic stimulation. In the control chamber, the dashed blue line indicates random optogenetic stimulation. **h,** In ChR2 rats, BMI treatment reduced aversion associated with mechanical allodynia in the SNI model. n = 6 rats; p = 0.0313, two-sided Wilcoxon signed-rank test. Data are presented as mean ± s.e.m. of biological replicates. **i,** YFP control rats demonstrated no preference for the BMI treatment. n = 4 rats; p = 0.6250, two-sided Wilcoxon signed-rank test. Data are presented as mean ± s.e.m. of biological replicates. **j,** CPA scores for BMI treatment in SNI-treated rats. n = 6 rats with ChR2 injection, n = 4 control rats with YFP injection; p = 0.0381, two-sided Mann-Whitney U test. Data are presented as mean ± s.e.m. of biological replicates.

Author Manuscript Author Manuscript Author Manuscript Author Manuscript

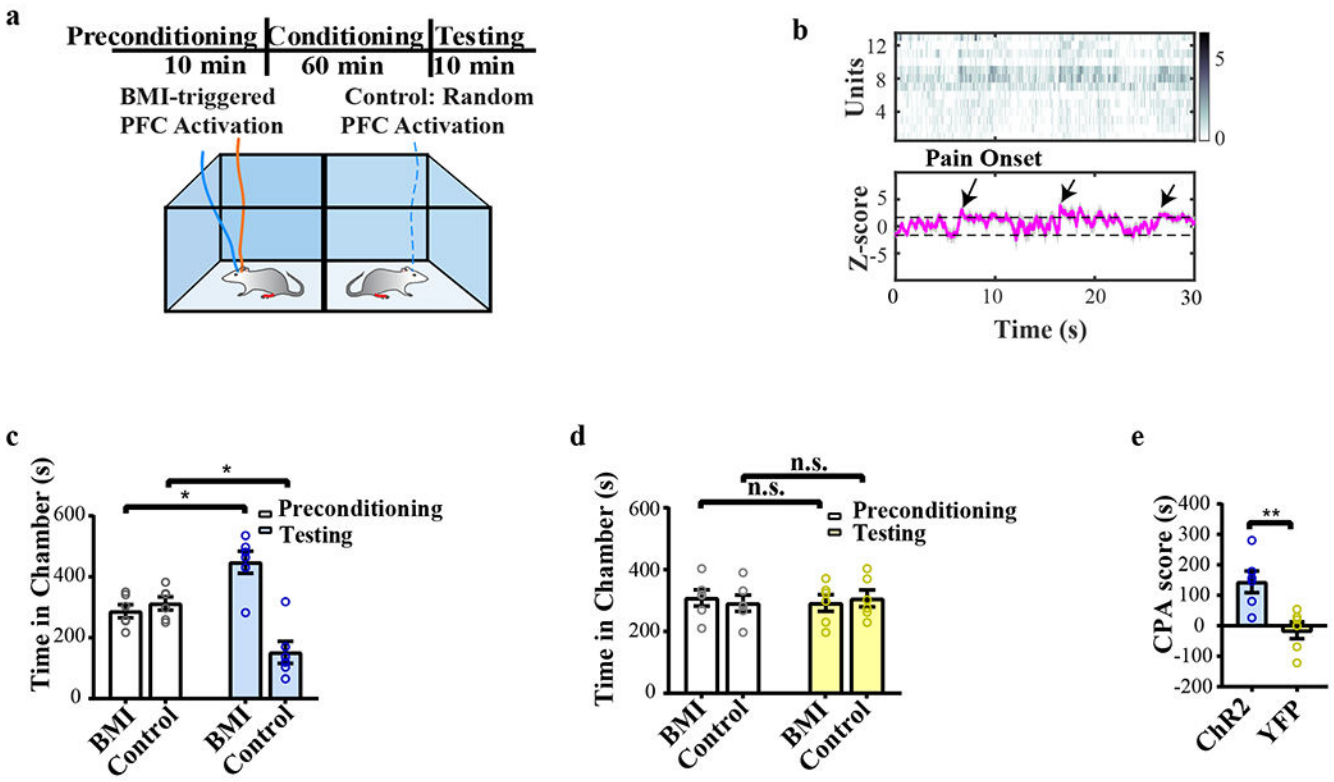

Fig. 6 |. Closed-loop BMI control of spontaneous pain in the chronic inflammatory pain model. **a**, Schematic of the CPA assay to test tonic or spontaneous pain in the CFA model. No peripheral stimuli were given. One of the chambers was paired with BMI, and the opposite chamber was paired with random PFC activation of matching duration and intensity. The orange solid line on the rat's head denotes BMI decoding, while the blue line denotes optogenetic stimulation. In the control chamber, the dashed blue line indicates random optogenetic stimulation. **b**, An example session of sequential pain onset detection based on the SSM-based decoder in a CFA-treated rat. The top raster plots show online sorted population spike counts (bin size =50 ms), with the darker color representing greater spike counts. The unit of color bar is spikes/bin. The bottom magenta trace represents the estimated Z-score from the univariate latent state, and the shaded area marks the 95% confidence intervals (CI). Horizontal dashed lines mark the significance thresholds (see Methods). The black arrows indicate detected onset of tonic pain episodes. n=13 biologically independent neurons. **c**, In ChR2 rats, CFA-treated rats prefer the BMI chamber. n = 6 rats; p = 0.0313, two-sided Wilcoxon signed-rank test. Data are presented as mean ± s.e.m. of biological replicates. **d,** YFP control rats demonstrated no preference for the BMI treatment. n = 6 rats; p = 0.8125, two-sided Wilcoxon signed-rank test. Data are presented as mean ± s.e.m. of biological replicates. **e,** CPA scores for BMI treatment in reducing tonic pain in CFA rats. n = 6 rats with ChR2 injection, n = 6 control rats with YFP injection; p = 0.0087, two-sided Mann-Whitney U test. Data are presented as mean ± s.e.m. of biological replicates.

Author Manuscript Author Manuscript Author Manuscript Author Manuscript

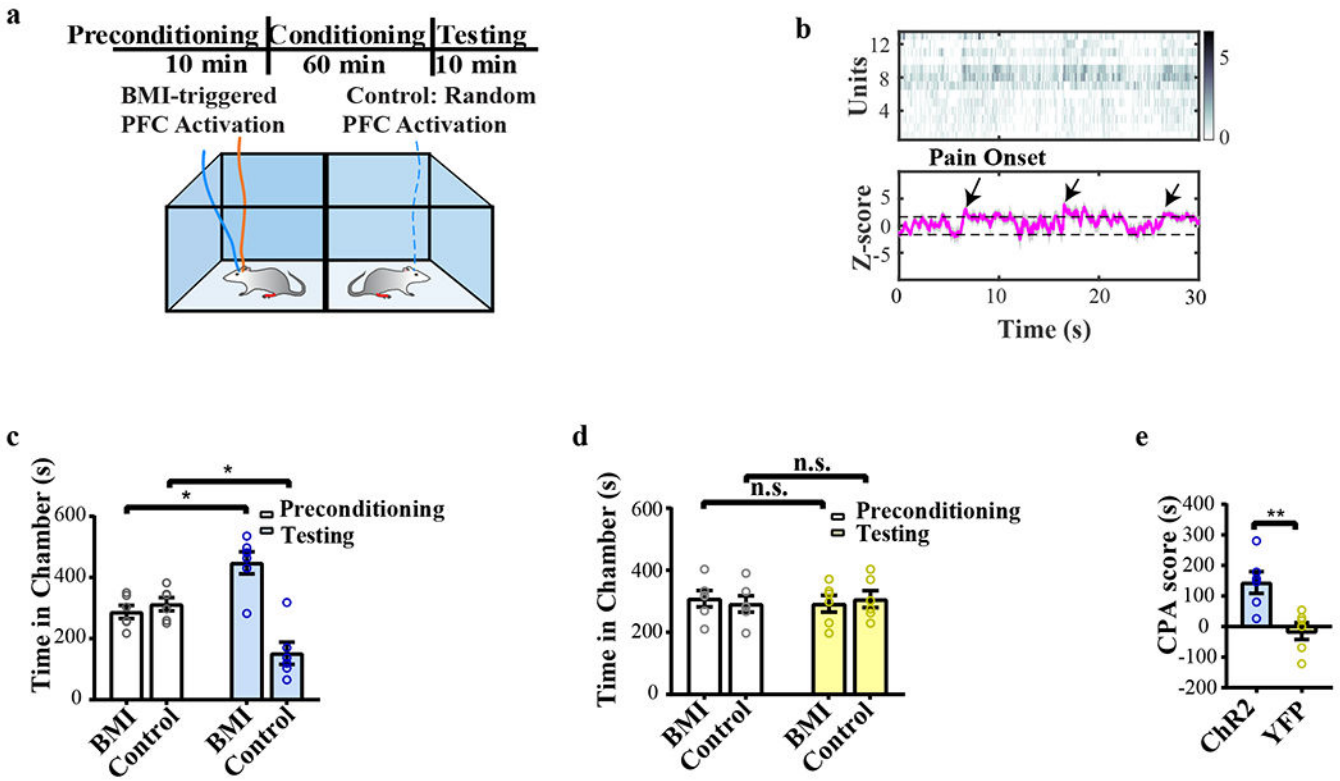

Fig. 7 |. Closed-loop BMI control of spontaneous pain in the chronic neuropathic pain model. **a**, Schematic of the CPA assay to test tonic pain in the SNI model. No peripheral stimuli were given. One of the chambers was paired with BMI, and the opposite chamber was paired with random PFC activation. The orange solid line on the rat's head denotes BMI decoding, while the blue line denotes optogenetic stimulation. In the control chamber, the dashed blue line indicates random optogenetic stimulation. **b**, An example session of sequential pain onset detection based on the SSM-based decoder in a SNI-treated rat. The top raster plots show online sorted population spike counts (bin size =50 ms), with the darker color representing greater spike counts. The unit of color bar is spikes/bin. The bottom magenta trace represents the estimated Z-score from the univariate latent state, and the shaded area marks the 95% confidence intervals (CI). Horizontal dashed lines mark the significance thresholds (see Methods). The black arrows indicate detected onset of tonic pain episodes. n=6 biologically independent neurons. **c**, In ChR2 rats, SNI-treated rats preferred the BMI chamber after conditioning. n = 6 rats; p = 0.0313, two-sided Wilcoxon signed-rank test. Data are presented as mean ± s.e.m. of biological replicates. **d,** YFP control rats demonstrated no preference for the BMI treatment. n = 4 rats; p = 0.8750, two-sided Wilcoxon signed-rank test. Data are presented as mean ± s.e.m. of biological replicates. **e,** CPA scores for BMI treatment in reducing tonic pain in SNI rats . n = 6 rats with ChR2 injection, n = 4 rats with YFP injection; p = 0.0381, two-sided Mann-Whitney U test. Data are presented as mean ± s.e.m. of biological replicates.